
Characterisation of Mycelial Morphology Using Image Analysis

Gopal C. Paul · Colin R. Thomas*

Centre for Bioprocess Engineering, School of Chemical Engineering
University of Birmingham, Edgbaston, Birmingham, B15 2TT, UK
E-mail: G.C.Paul@bham.ac.uk; C.R.Thomas@bham.ac.uk

Image analysis is now well established in quantifying and characterising microorganisms from fermentation samples. In filamentous fermentations it has become an invaluable tool for characterising complex mycelial morphologies, although it is not yet used extensively in industry. Recent method developments include characterisation of spore germination from the inoculum stage and of the subsequent dispersed and pellet forms. Further methods include characterising vacuolation and simple structural differentiation of mycelia, also from submerged cultures. Image analysis can provide better understanding of the development of mycelial morphology, of the physiological states of the microorganisms in the fermenter, and of their interactions with the fermentation conditions. This understanding should lead to improved design and operation of mycelial fermentations.

1	Introduction	2
2	Image Analysis Systems	4
2.1	Hardware	5
2.2	Software	7
2.2.1	Image Acquisition	7
2.2.2	Grey Scale Processing	7
2.2.3	Object Detection	10
2.2.4	Binary Image Processing	10
2.2.5	Image Editing	13
2.2.6	Measurements and Calculations	13
2.2.7	Data Analysis	13
3	Image Analysis Methods	15
3.1	Dispersed Morphology	18
3.1.1	Sample and Slide Preparation	19
3.1.2	Setting Up of Image Analysis Parameters	20
3.1.3	Image Analysis Software	20
3.2	Pellet Morphology	29
3.2.1	Sample and Slide Preparation	30
3.2.2	Image Analysis Parameters	30

* To whom all correspondence should be addressed.

3.2.3	Image Analysis Software	30
3.3	Fungal Spore Germination	35
3.3.1	Sample and Slide Preparation	36
3.3.2	Image Analysis Parameters	36
3.3.3	Image Analysis Software	37
3.3.4	Measurement	40
3.4	Hyphal Differentiation	45
3.4.1	Sample and Slide Preparation	45
3.4.2	Setting Up of Image Analysis Parameters	46
3.4.3	Image Analysis Software	46
4	Conclusions	58
5	References	58

1

Introduction

Many important industrial fermentation processes utilise filamentous micro-organisms such as fungi and *Actinomycetes* for production of commercially important products, including most antibiotics, and some enzymes and organic acids, in addition to microbial biomass itself which is used in some foodstuffs. The growth of filamentous microorganisms is more complex than that of unicellular bacteria and yeasts. The development of the filamentous form usually starts from the germination of a spore, the germ tubes of which are progressively transformed into mycelia, i.e. networks of hyphae, through hyphal extension and branch formation. A fungal or *Actinomycete* hypha may be up to several hundred microns long and is typically 3–10 µm in diameter for fungi and 0.5–1.5 µm for *Actinomycetes* [1].

The filamentous form of growth allows the organism to increase in size without altering the protoplasmic volume: surface area ratio, which makes these microorganisms well adapted to colonisation of solid substrates [1]. However, for economic production, most processes require submerged culture in large fermenters, often with intense agitation and aeration. Under these conditions, a wide variation in gross morphology (shape) is found, varying from discrete or loosely entangled filaments, the dispersed form, to pellets (spherical colonies of highly entangled hyphal mass). In many cases, productivity seems to depend on morphology [2, 3]. In addition, the dispersed form of growth can lead to hyphal entanglement in the fermentation broth. This type of morphology at high biomass concentration can lead to an adverse effect on the rheological properties of the broth, making it highly viscous and pseudoplastic, and thus difficult to mix in a large fermenter, so that inhomogeneities may arise. Furthermore, oxygen transfer from sparged air bubbles to the microorganisms decreases with increasing viscosity. In severe cases, this can lead to oxygen limitation. Heat transfer for fermenter cooling may also be reduced under such conditions. Such problems can lower productivity. They cannot always be overcome

by the use of high agitation speeds because of the potential "shear" damage to mycelia, also with adverse effects on productivity. Rheological problems are less with the pelleted forms, but the centres of large pellets might be starved of oxygen and autolyse, again affecting productivity. Clearly the morphology of these filamentous microorganisms is a matter of profound concern for fermentation scientists.

Other types of structural variation can also occur in filamentous micro-organisms. Some fungi and all *Actinomycetes* are septate (i.e. they have cross-walls which divide the hyphae into a series of compartments). As growth occurs only at the hyphal tips [1], these hyphal compartments vary greatly in age and in physiological state, and can show various forms of structural and biochemical differentiation [4–8]. For example, vacuoles can appear in the hyphae during later stages of growth (Fig. 1). In general, the further the compartment is from the apex (i.e. the older the compartment), the larger the vacuoles. Hyphal vacuolation has been used to quantify the physiological structure of fungal biomass [7, 8] and has been related to antibiotic production from *Streptomyces spectabilis* [9] and *Penicillium chrysogenum* [10]. The expression of genes associated with secondary metabolic activities such as antibiotic production might be related to the process of differentiation.

Morphology and differentiation are often studied using microscopy, which yields either qualitative information, or quantitative information through labour-intensive and sometimes subjective analysis by the observer. The power of image analysis lies in extracting quantitative information from such observations in a reproducible, (semi-) automated manner. A semi-automatic image analysis for characterising mycelial morphology was developed in 1988 [11]. Since then, the power and capability of image analysers have been increasing rapidly, and so have the applications in this area. Image analysis methods have been reported for automatic characterisation of mycelial morphology [12, 13]

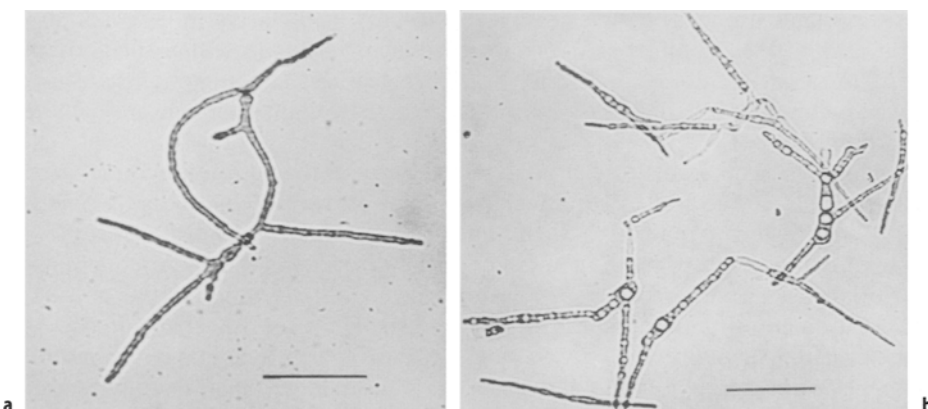


Fig. 1 a, b. Vacuolation of *P. chrysogenum* mycelia in fed-batch fermentation. Photograph of mycelial during: a the rapid growth phase (15 h); b the production phase (87 h). Bar length = 40 µm

and pellet structure [14]. Automatic image analysis has also been reported for characterising swelling and germination characteristics of fungal spores in inoculum fermentations [15]. Substantial evidence suggests that the quality of the initial spore preparation (e.g. spore age, concentration) and medium conditions can influence subsequent mycelial growth, morphology and productivity [3, 15, 16]. Recently an image analysis method has been developed to characterise hyphal vacuolation [7] and a method for the simple differentiation of *P. chrysogenum* is now available [8]. The resulting quantitative information about the biomass structure has permitted a powerful structured model for the penicillin fermentation to be built [17].

Many of these applications of image analysis were reviewed by Thomas [18]. A broader review of image analysis applications in biotechnology has been published by Vecht-Lifshitz and Ison [19] and more recently a review on applications of image analysis in cell technology has been published by Thomas and Paul [20]. The present work provides detailed descriptions of the main methods used to characterise mycelial morphology and differentiation. A complementary discussion concerning staining and more detailed physiological characterisation of *P. chrysogenum* can be found in Chap. 2 by Pons and Vivier.

2

Image Analysis Systems

A typical image analysis system consists of a personal computer (PC) or a work station, sometimes with specialised dedicated hardware, which can capture an image or picture and can be programmed to extract information from the image or to enhance features of interest within it, such as microorganisms. The source of the image is usually from a camera mounted on a microscope or from another video source or an electron microscope. The image is digitised in the computer both in space and tone to produce an array of picture elements or "pixels". A typical image consists of 512×512 pixels, each of which usually has one of 256 possible greyness (brightness) levels usually in the scale of 0=black and 255=white. Most applications work with monochrome images where brightness differences are exploited to distinguish critical features. Colour systems are also available, but their handling requires more expensive equipment and specialised software.

For microscopic work, image analysis has become an invaluable accessory for obtaining accurate and quantitative information from microbial samples. There is a wide variety of manual and semi-automatic alternatives available. Measurements using a manual method might be either direct from the microscope stage with the aid of micrometers, or indirect from photographs of the objects. Measurements on photographic images are usually made with a ruler or micrometer gauge or indirectly from tracings or drawings obtained by outlining the images with a marker. To increase speed the photomicroscopic method has also been combined with the use of an electronic digitiser attached to a computer [21]. With complicated objects more sophisticated measurements are necessary. Furthermore, studies on microorganisms often involve the measurement of hundreds of objects to obtain statistically sensible results. Such large numbers of

measurements are too tedious to collect by manual means, and image analysis is often preferable, especially as it can easily be (semi)automated. Adams and Thomas [11] proposed the use of such semi-automatic image analysis for characterising the morphology of mycelial cultures. They compared their image analysis method with the electronic digitising method used by Metz et al. [21], using *Streptomyces clavuligerus* samples from submerged cultures. It was shown that the semi-automatic method is more precise and faster than the digitising method. An additional advantage of image analysis is its application of strictly consistent criteria to measurements, which should be independent of the operator. This can remove most of the subjectivity and inconsistency associated with manual methods. Finally, some measurements can also be considered with image analysis that would otherwise be unrealistic, or too costly.

An image analysis system consists of two major components: hardware and software, and these are discussed in the following sections.

2.1

Hardware

The basic hardware components of image processing systems are: input devices (microscope, macroviewer or similar device with a video camera attached; video recorder; scanner; etc.), and a high performance personal computer or workstation with optional image processing microprocessors. Additional items may include a mouse, light pen or joystick, a massive storage device, and normal and/or video printers. For automatic operation using a microscope, this should be fitted with a motorised stage, a controllable illumination system, and autofocus capability. Figure 2 shows the elements of image analysis systems which can be selected to give varying degrees of sophistication.

A motorised stage allows scanning of a microscope slide. An extra large automated stage can be loaded with several slides to allow extended operation. Field brightness can be controlled by a lamp controller using the video signal from the

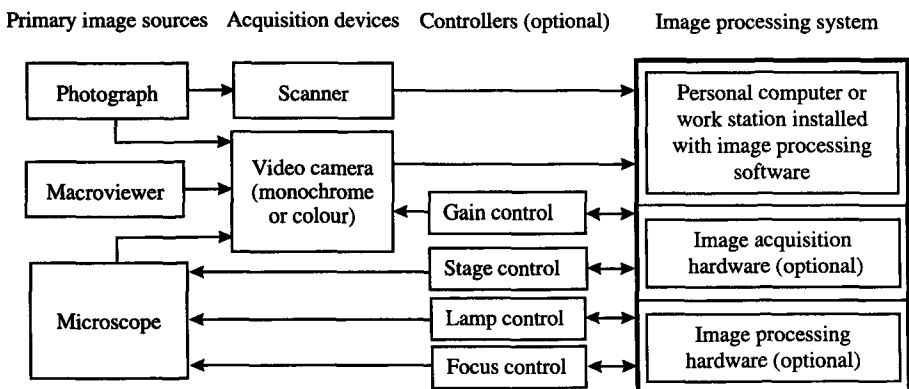


Fig. 2. Hardware components of typical image analysis systems

camera to control the lamp brightness. An automatic focus actuator is usually used in conjunction with the motorised stage where normal variations in surface height of the sample will cause the specimen to move out of focus on scanning.

Different types of devices such as video cameras and scanners are used in image acquisition. There has been a recent specialised review on different types of image acquisition devices and their general characteristics with respect to their use in advanced image analysis work [22]. Such devices translate video images or photographic images into electrical signals with amplitude proportional to the image brightness at any given point. A scanner perform a point-by-point scan from a picture to produce an array of spots representing the original picture. Scanners are usually attached to host computers, i.e. they do not include specialised hardware to acquire images rapidly. Advanced image processing systems use two main types of video camera: tube cameras and solid-state charged coupled device or CCD cameras. Tube cameras are older but they are still used for their high sensitivity especially for applications in fluorescence and luminescence (intensified cameras) where the light levels are very low. The CCD cameras are easier to use and are becoming more and more available at affordable prices. The analogue signal from either type of camera is converted to digital format by a high speed analog to digital converter (ADC) to give discrete grey levels. Usually the ADC converter is built into the image analysis hardware. Most video cameras produce square pixels (or picture elements) but some give rectangular or quasi-square pixels. In the final discretisation which takes place in the image analysis hardware such rectangular or quasi-square pixels are usually corrected to give square pixel based images. In an image the larger the size of the array, the higher the resolution, and the finer the spatial details that may be detected. It is of course necessary to match as closely as possible the array size of the camera and that of the image being handled by the image analyser. Usually 256×256 to 1024×1024 arrays of pixels are common. Other dimensions such as 768×576 pixels based images are also available; these reflect camera technology.

The digitised image can now be processed to extract the desired information. Several features of image processing operations are primarily due to the large memory requirements for handling and processing images. For example, a typical digital image consists of 512×512 pixels. Each pixel, having 256 possible greyness levels, can be encoded in a byte. This means that to store the image 262144 bytes are required. A colour image is composed of three monochrome images (representing the red, green and blue) and therefore requires three times as much memory. Besides the large amounts of memory needed, even applying a simple image processing operation to an image may require several arithmetic operations for each pixel, which could easily amount to over 100 million processor operations for the single operation. This requires fast hardware for good performance. Many commercial image analysis systems now use dedicated hardware where the image processing is undertaken by a special microprocessor designed for speed.

A fast PC or a workstation installed with image analysis software is cheap but has limited abilities and speed. With additional dedicated image processing

hardware the system can be more functional in terms of power and speed but becomes more costly. To base the complicated or time intensive operations on hardware, and the relatively simple operations on software relying on the host central processing unit (CPU) speed, is an acceptable compromise for some applications. This could be an attractive approach, particularly to fermentation technologists or microscopists who still rely on manual methods, and who also need a cheap route to image analysis. The rapid increase of CPU speed of PCs and workstations and the reduction of overall computer costs is expected to encourage many commercial firms to take advantage of these developments to provide more affordable solutions to image analysis problems. On the other hand, high performance systems consisting of on-board hardware and a library of functions for image processing also implemented in hardware allow complicated applications to proceed at high speed, saving the operator time and permitting more rapid research progress.

2.2

Software

Software is a vital element of an image processing system. It consists of programs that control the hardware to carry out a variety of enhancement, manipulation, filtering and smoothing operations, and measurements. Software provides the users with a set of tools which can be applied to develop a program appropriate to a particular application. The required sequence of image processing operations can be encoded in such a program to allow fully automatic repeatable analysis and measurements. Most image processing packages have been designed for application developers rather than the final users and the image analysis routines come as a library supported by a common programming language.

A number of distinct steps are involved in image analysis applications: image acquisition, grey image enhancement, image detection, binary image processing, image editing, measurements and calculations, and data analysis. Some of the functions are described briefly here, and will be referred to in describing specific applications in Sect. 3. More detailed explanations can be found in the thesis by Paul [23].

2.2.1

Image Acquisition

Image acquisition covers selection of fields of view, microscopic magnification, and adjustment of lamp brightness and focus to give sufficient contrast to enable the image analyser to identify the objects of interest. Finally the image is captured into digital form ready for processing.

2.2.2

Grey Scale Processing

There are a large number of image processing functions available to improve the quality of grey images. Each involves a grey scale transformation where the grey

level of each pixel is transformed to another value using rules that take into account the original values for that pixel and its neighbours, or its spatial relationship to many other pixels. Sometimes images may be subtracted or added together to remove some spurious artefacts or to improve images that are poor in quality. There are certain filtering techniques that select only some kinds of image data, for example edges and boundaries.

Grey processing operations can be divided into two categories: point operations and neighbourhood operations. Point operations are performed on individual pixels. For instance, if the original greyness values covered only a small fraction of the total range available, then new values covering the whole range could be substituted pixel by pixel to increase the image contrast. Neighbourhood operations are carried out on groups of adjacent pixels. For example each pixel in a square array is surrounded by eight neighbours. Such a group of pixels is known as a "structuring element" (SE). SEs are often square but could be other shapes. By setting the central pixel greyness of a square SE, using its neighbours' greyness values and applying some rules relating the former to the latter, changes in intensity across small parts of the image can be achieved, e.g. for smoothing or to remove noise from an image. The terminology most often used to describe these operations is "morphological transforms". In "mathematical morphology" [24] the relationship between the value of each pixel and that of its neighbours is expressed in logical terms, using AND and OR for binary images and "greater than" and "less than" for grey images. The particular grey scale transformation functions used in a number of applications discussed in Sect. 3 are described briefly here.

"Erosion" and "dilation" are the most common morphological operations used to process both grey images and binary images. In grey erosion the pixels covered by the SE are examined for the one with the lowest numerical value. The central pixel in the SE is set to this minimum value in the output image. This produces two effects: first, the resulting image becomes darker than the original image; and second, any brighter details that are smaller than the SE are eliminated. Exactly opposite effects are observed in grey dilation, i.e. the maximum value covered by the SE is chosen and copied to the output image. By this operation the general brightness of the output image is raised and dark details are removed.

These two basic functions are used to build a large number of secondary functions designed to extract or separate details in a grey image. "Delineation" and "top hat" are two highly useful functions. Delineation selects a local minimum or maximum grey value of neighbouring pixels by a combination of erosion and dilation operations. This improves the contrast of a grey image particularly around object boundaries (see for example applications described in Sects. 3.1 and 3.2). Figure 3 shows the grey level variations across an object boundary before and after the delineation operation. By a top hat operation either the white details (using "white top hat") or dark details (using a "black top hat") can be extracted from an image. For example, this function has been used to extract halos from around hyphae in an image (Sect. 3.4). Figure 4 illustrates how halos around an object's boundaries can be extracted using the white top hat operation.

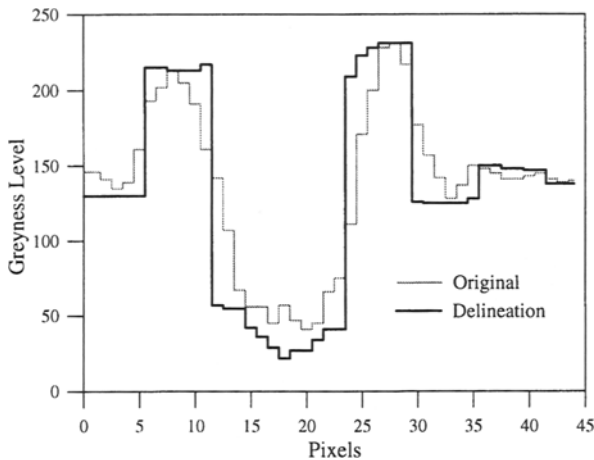


Fig.3. Effect of delineation on a grey level profile

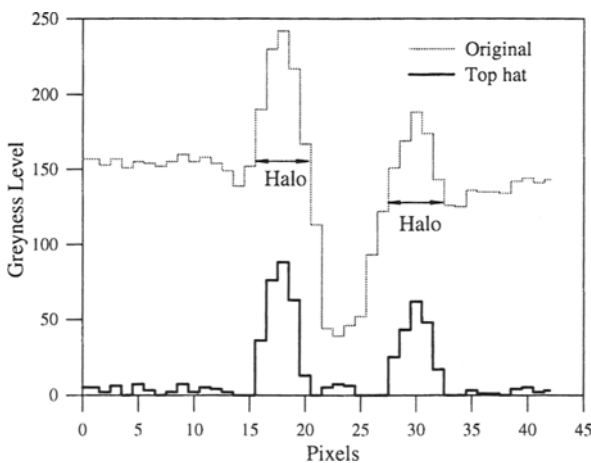


Fig.4. Extraction of white details (e.g. halos) across object boundaries using the white top hat operation

A complex grey image sometimes contains many features touching each other at numerous points, and the zone of influence corresponding to each feature may not be easily distinguishable or separable. A “watershed” is a grey transformation which is often used to separate features from such images. The watershed segments a grey image into its “catchment basins”. A grey image can be seen as a topographic surface. According to the law of gravitation, if a drop of water falls on such a surface, it will run down a hillside until it reaches the sea or a lake. All places from which such a drop will reach a given lake are in that lake’s catchment basin. If a grey image is considered to be a topographic surface with height represented by the greyness level of any given pixel, a watershed will find

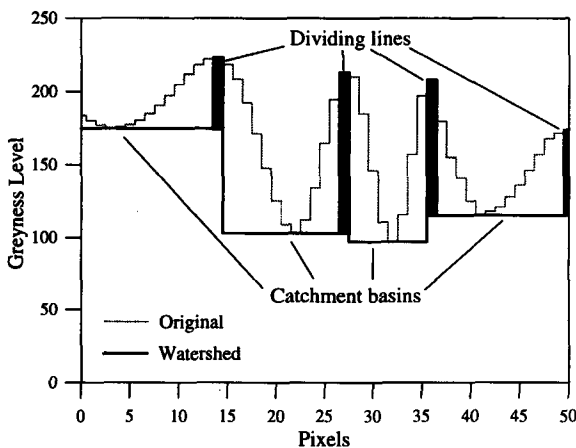


Fig. 5. Watershed of a grey profile. Local minima are expanded until the dividing lines are reached

the catchment basins or regional minima of the surface. This process highlights the ridges or “watershed lines” (also called “dividing lines”) separating the various zones of influence (the basins). Figure 5 shows the effects of a watershed operation on a grey profile. This operation has been used to separate closely spaced regions in hyphae (stained and non-stained regions), as discussed in Sect. 3.4.

2.2.3 *Object Detection*

Detection is the stage in the image processing sequence which attempts to identify and separate the objects requiring processing from the rest of the image. Detection is achieved by setting threshold levels of greyness corresponding to the greyness levels of the regions of interest. The result of applying this process to a grey image is to create a simpler binary image, which has only two values, everything that is selected is “white” and the rest is “black”. This is a data reduction step as these images contain less information than grey ones. However, they are smaller and therefore need less computer memory, and processing on binary images is much faster than on grey images. If the extra information in the grey image is not required, then detection is a useful operation.

2.2.4 *Binary Image Processing*

The binary image may not perfectly represent all the objects required. This may be due to noise or other imperfections in the original image, to inadequate processing methods, or sometimes to features inherent in the image itself such as

touching objects. Normally, these kinds of situations are dealt with by manipulating the binary images to improve their quality or to achieve object separation, for example, using binary "erosion" or "dilation" operations to smooth object outlines, join broken or discontinuous objects, and to separate touching ones.

By a binary erosion operation a layer of pixels is removed from the boundary of the object in the binary image. Narrow protuberances on objects are removed, and objects connected by a narrow strand have that removed by this operation. Dilation is the reverse of erosion, causing features to grow in size by the addition of pixels at the boundary, which fills in small breaks, internal voids, or small indentations along the object edges.

Erosion and dilation may sometimes be used in tandem. The sequence of erosion followed by dilation is called an "opening". The initial erosion removes

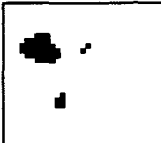
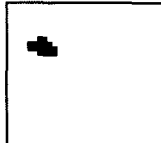
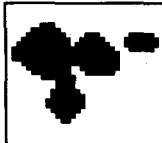
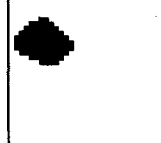
Binary image			
Operations	First step	Second step	Third step
Erosion			
Dilation			
Opening			
Closing			

Fig. 6. Expanded view of binary erosion, dilation, opening and closing operations

small features which may represent noise, and also sharp protuberances. The subsequent dilation cannot restore these small features, which have permanently disappeared, but does fill in any small indentations in the outlines. The overall result is that the object size (number of pixels) is restored to nearly its original value, while the shape is modified to become more rounded, smooth and less noisy. When the sequence is reversed (i.e. dilation followed by erosion) it is referred to as "closing". In some respects it is the opposite to opening, because small features are not erased. Small voids in objects are still filled in, and breaks or gaps are joined. Multiple applications of opening and closing produce more extreme smoothing or shape modification, and more complete removal (in opening) or joining (in closing) of objects. Figure 6 illustrates by diagrammatic presentations how erosion, dilation and the derived functions opening and closing operate on different types of objects and the features attached to each.

One of the most interesting specialised uses of erosion is "skeletonisation". The skeleton consists of the lines of pixels that mark the midlines of an object. When the object has branches or projections, this technique can be used to find the number of branches or nodes and to describe the amount of branching in the object. There are other applications for which the skeleton is useful. Different skeletonisation operations and their applications have been described by Russ [25]. Figure 7 shows the skeletonisation operation on branched objects. Very often skeletonised objects may contain many branches which may represent actual branches or may be caused by extraneous touching particles or detection irregularities. To reduce these another function called "pruning" is used. This shortens the skeleton by peeling away the ends until false branches have been removed. Multiple use of this function may cause complete disappearance of branches. There are some other functions used to find the characteristics of the skeleton, e.g. to identify the end points (useful in counting the number of tips in a hypha), the joining points or the triple points.

There are other binary processing functions which are also useful in many applications, e.g. "filling", "segmentation", "geodesic rebuild". Through a filling

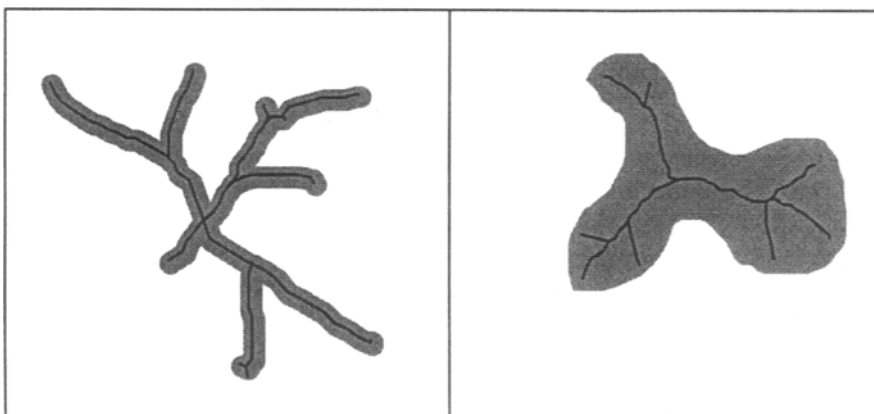


Fig. 7. Skeletonisation of binary image to obtain branches

operation the internal voids or holes of an object are filled (without affecting the outer boundary) giving a solid object. The segmentation operation is applied to separate touching objects which involves many iterations of binary erosion and dilation operations with reference to a map of greyness level variations of the original grey image. Many alternative algorithms have been proposed for obtaining the best separation [25, 26]. A geodesic rebuild is the reconstruction of an object by dilation of “seeds” or markers within the object until it corresponds with a mask of the original object. Objects without seeds cannot be rebuilt. This operation is often used after eroding away smaller objects in order to restore larger objects to their original shapes and sizes without reintroducing the smaller ones. If the smaller objects are desired, they can be found later by image subtraction.

2.2.5

Image Editing

The final image produced after complete (or a stage of) processing may contain false details and other unwanted objects which cannot be identified. It can then become desirable to modify the image manually before final measurements or before another stage of image processing is started. Using edit functions the operator can modify the image to:

- specify particular regions of interest;
- correct object details, e.g. draw in a partially or completely missing feature;
- reject unwanted regions of an object or a whole object;
- separate touching features or objects.

2.2.6

Measurements and Calculations

Four types of parameters can be obtained from image measurements: size, shape, position, and grey scale (brightness) information. Within each of these categories, there is a variety of individual parameters that can be measured or calculated from others. Table 1 summarises some of the parameters that are most often used in applications like characterising mycelial morphology, spore germination and differentiation.

2.2.7

Data Analysis

Once the measurements and calculations have been made, the data can be classified and analysed to give the final results, which might be in tabular form, graphical or might be stored in a file to be processed later using stand alone statistical or other software.

Table 1. Some important parameters obtained by image analysis

Parameters	Definition/Formula
<i>Object size:</i>	
Area or projected area (A)	Area of the projection of a 3-dimensional object into a two-dimensional image. This is often found by a pixel (picture element) count, but is expressed as an actual area by multiplying by a calibration constant squared
Perimeter (P)	Length of the boundary of an object. As pixels lie on a rectilinear grid, it is necessary to include diagonal inter-pixel distances where appropriate, otherwise a square and its inscribed circle would appear to have the same perimeter
Convex perimeter (P_C)	Length of the perimeter obtained by joining the outer points of an object, i.e. by filling in all the concavities in an object
Convex area (A_C)	Area inside the convex perimeter.
Length or fibre length (L)	The length of a rectangular object having the same area and perimeter as the measured object. This is derived from area and perimeter as
	$L = \frac{P + \sqrt{P^2 - 16A}}{4}$
Width or fibre width (W)	The width of a rectangular object having the same area and perimeter as the measured object. The width of an object is derived from area and perimeter as
	$w = \frac{P - \sqrt{P^2 - 16A}}{4} \text{ or } w = \frac{A}{L}$
Equivalent circular diameter (D)	The diameter of a circle having the same area as the measured feature. Derived from area as
	$D = \sqrt{\frac{4A}{\pi}}$
Breadth and height	These parameters are obtained by feret measurements. A feret is equivalent to a diameter measured using a pair of callipers. Breadth gives the length of the shortest feret and height the longest feret
Maximum distance	The longest feret across the convex area of a mycelial particle gives the maximum distance. This parameter is used to characterise a mycelial clump
<i>Object count:</i>	
No. objects	Number of objects per field of view and cumulative counts for a sample

Table 1. (continued)

Parameters	Definition/Formula
Hyphal tips	Number of tips per hypha, mean number of tips per hypha for a sample
<i>Object shape:</i>	
Circularity (C)	A shape factor describing the deviation of an object in an image from a true circle. This is derived from area and perimeter $C = \frac{P^2}{4\pi A}$
	This gives a minimum value of 1 for a circle, larger values for shapes having a higher ratio of perimeter to area
Roughness (R)	A measure of the irregularity of the perimeter of an object. It is obtained from the circularity measurement around an object boundary
Compactness or fullness (F)	This is a measure of the voidage of a particle and is used to characterise mycelial clump and pellet structure. It is the ratio of the actual area of the particle to the convex area. For a pellet without hairy regions $F \approx 1$, and for a loose clump $F < 1$
<i>Object position:</i>	
Coordinates (X,Y)	x-coordinates, y-coordinates, often implemented with the origin at the pixel
Feature count point (X-FCP,Y-FCP)	The FCP is the last rightmost pixel of the lowest scan line contained in the object. FCP with a guard frame is used to avoid object truncation in automatic methods
<i>Object brightness:</i>	
Grey intensity (G)	A measure of the brightness of a part of the image. Two types of grey intensity are used: mean grey intensity (MG) giving the mean of grey levels of pixels overlaid by a binary feature and integrated grey intensity (IG) giving the sums of the grey levels of pixels overlaid by a binary feature

3

Image Analysis Methods

This section describes four main image analysis applications in fermentations using mycelial microorganisms. The image analysis methods were developed on a Quantimet 570 image analyser (Leica Cambridge Ltd, Cambridge, UK. – see Fig. 8). The Quantimet 570 is a general purpose image processing and analysis



Fig. 8. Photograph of the Quantimet 570 image analysis system

system consisting of a Motorola 68000-based monitoring unit, supervising a morphological processor unit, graphic overlay and binary image memory, a measurement processor, the acquisition and display system, and peripheral control interfaces. An 80486-based PC host computer serves as the user's interface. The overall image processing speed of the Quantimet 570 has been improved by incorporating programmable logic cell array technology, based on concepts of mathematical morphology, into the morphological processing unit [24]. A Polyvar II optical microscope (Reichert Jung, Optische Werke AG, Wien, Austria) fitted with a colour 3CCD camera (Model XC-007, Sony, Japan) and macroviewer (supplied by Leica Cambridge Ltd) fitted with a CC-TV monochrome camera (Sanyo Electric Co. Ltd, Basel, Switzerland) were connected to the image analyser. For automatic operation the microscope was fitted with an eight-slide motorised stage (supplied by Leica Cambridge Ltd), a controllable illumination system, and autofocus capability. The stage is drivable in 3-dimensions with a 2.5 μm step size in the x - y directions for scanning on the microscope slide and a 0.05 μm step size in the vertical direction for automatic focus control.

The image analysis routines have been implemented on the Quantimet 570 by means of its interactive basic programming environment, QBASIC, or using a C compiler and its image processing library, ADSOFT 1.01 (Advanced Software Developer's Kit, Leica Cambridge Ltd, Cambridge, UK). ADSOFT consists of a C library of commands to control stage utilities (e.g. initialisation, scanning, and autofocus), lamp brightness, and the image processing hardware. The image processing library consists of an extensive range of grey, binary, and colour image processing routines (including those described already in Sect. 2.2) and facilities for image measurements. All the programs described here were initially

developed using QBASIC [7, 13–15]. Except for the pellet program described in Sect. 3.2, all were then extended and enhanced [8, 27, 29] using C and C⁺⁺ (Borland Inc., Scotts Valley, CA, USA) and ADSOFT. Although the routines were developed on the Quantimet 570, they ought to be implementable on other systems. However, the resulting performance will largely depend on the image processing hardware and the image acquisition optics used.

Image analysis begins with specimen preparation. In most cases, the specimen is carefully prepared for optical microscopy in order to achieve optimum image quality and ease of analysis. The fermentation samples are often diluted and shaken to disperse the mycelia, pellets, or spores, and stained to enhance the contrast of the microscopic images. Many methods use a special stain [8] or a number of stains to pick out hyphal regions of interest. This is described further in Sect. 3.4. Slide preparation needs to be performed carefully to avoid inclusion

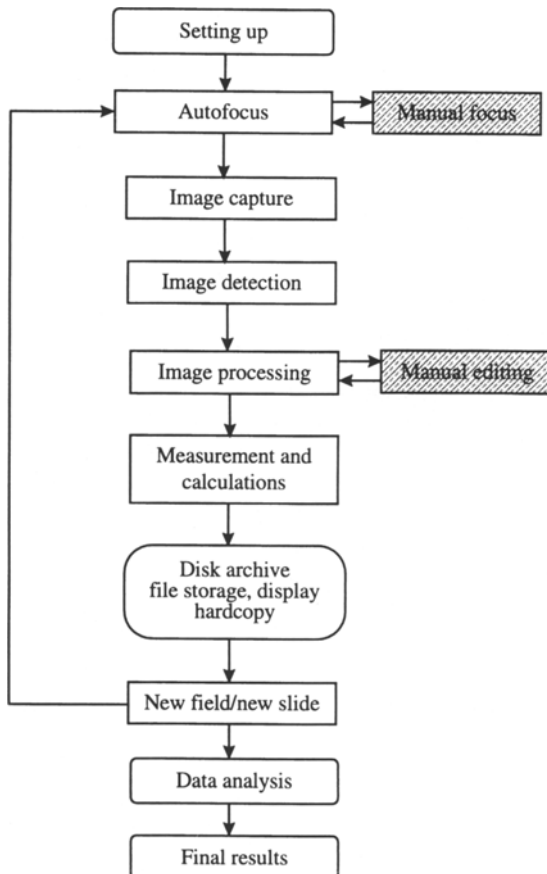


Fig. 9. General structure of the software used for automatic and semi-automatic image analysis. Semi-automatic image analysis uses manual focus adjustment and manual editing

of many possible artefacts, e.g. dirt, air bubbles. Bad slide preparation can make subsequent image analysis more difficult and increase the load of operator time through requiring unnecessary manual editing of images.

All the image analysis routines presented here follow the general structure shown in Fig. 9. A routine consists of seven phases (some of which were described in Sect. 2.2): setting up, image acquisition, grey image processing, image detection, binary image processing, image measurement and data analysis. Grey and binary image processing stages consist of a combination of image processing operations, chosen to achieve a particular result; therefore these vary with the application. Detailed descriptions of these application-specific phases are given in Sects. 3.1–3.4 below.

Each program requires two types of parameters to be set by the user: (a) hardware parameters, and (b) image processing parameters. The setting up for the hardware parameters include the microscope lamp brightness, autofocus parameters, the calibration factor for the objective to be used, and control parameters for automatic microscope stage movement (number and position of slides and total number of fields in each slide). During setting up, correction for uneven slide illumination “shading correction” can also be established, and the manual editing option selected if desired. Finally an active measuring frame might be set up to prevent bias due to truncation of objects at the image edge. The image processing parameters vary with the type of application and are therefore described separately. The setting up phase is required only once for each set of measurements. During analysis the whole sequence is then executed in repeated cycles until all the selected slides and fields of view have been analysed.

3.1

Dispersed Morphology

Adams and Thomas [11] developed a semi-automatic image analysis method for characterising the dispersed morphology of *S. clavuligerus* and *P. chrysogenum* samples from submerged fermentations. A similar method used to study the mycelia of *S. tendae* in a growth chamber mounted on a microscope stage was developed by Reichl et al. [28]. As this method was not intended for studying samples taken from submerged fermentations, it will not be discussed further. Subsequently an automatic method was proposed by Packer and Thomas [12] and this method considered mycelial clumps for the first time. These are loose aggregates of hyphae, which are not sufficiently tightly packed to be described as pellets, but which do not show a simple mycelial tree shape (see Fig. 10). Although the method of Packer and Thomas [12] gave the proportion of clumps as a percentage of the biomass in a sample by projected area, no further attempt was made to characterise the clumps. A fully automatic method has recently been published by Tucker et al. [13]. This latter method provided detailed analysis of mycelial morphology from non-pelleted cultures and included parameters to characterise clump structure in addition to the proportion measurement obtainable by the earlier method [12]. The method of Tucker et al. [13] has been further improved [29] and has been applied to a wide range of morphological forms from submerged *Actinomycete* and other mycelial

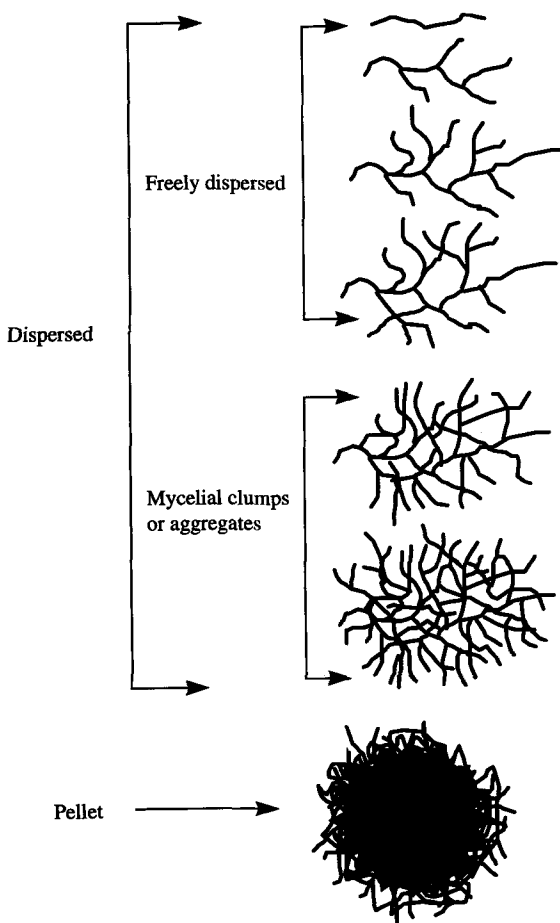


Fig. 10. Classification of mycelial morphology by image analysis

fermentations. It is described in more detail below. It does not characterise pellets and a separate method for this purpose is presented in Sect. 3.2.

3.1.1

Sample and Slide Preparation

Samples from fungal fermentations were fixed with an equal volume of fixative containing 13 ml 40% formaldehyde, 5 ml glacial acetic acid and 200 ml 50 vol. % ethanol. Before slide preparation the fixed sample was diluted with 20% (w/v) sucrose solution to prevent quick evaporation during analysis and stained with a few drops of lactophenol cotton blue (Fluka Chemika-BioChemika, Dorset, UK). The biomass concentration after dilution was usually kept below 1.0 g/l. The diluted sample was then placed on a slide and covered with a cover slip. The magnifi-

cation was typically in the range of $\times 40$ to $\times 100$. For *Streptomyces* spp. the Gram-staining method was usually used. The diluted sample after spreading on a slide was air-dried and then fixed over a hot Bunsen flame. The fixed mycelia were stained either by methylene blue or crystal violet. The unabsorbed stain was washed off with water and then the slide was left to dry. The magnification used was $\times 100$.

3.1.2

Setting Up of Image Analysis Parameters

Before images analysis was begun, various parameters had to be set. The setting up of the hardware related parameters has been described earlier. The image analysis parameters used for measuring hyphal morphology are listed in Table 2. These parameters are application specific, varying for the particular fermentation being investigated. The total number of mycelial particles to be measured typically varied from 150 to 250 and the time of analysis for one sample varied between 1 and 2 h.

3.1.3

Image Analysis Software

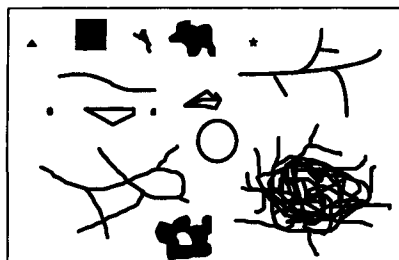
In the analysis phase the stage moved to the first position on the slide and then either an autofocus was performed or the user was prompted to adjust the fine

Table 2. List of image analysis parameters used for hyphal morphology analysis and their typical values used for different filamentous species

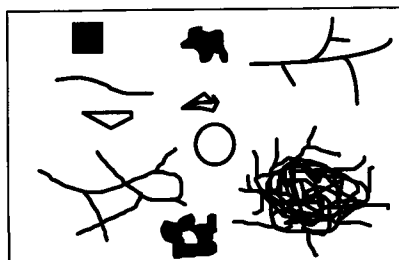
Parameters	Use in analysis stage	Value ranges	
		Filamentous fungi	Actinomycetes
Minimum branch length, μm	Minimum acceptable branch branchessize, to eliminate false touching debris	4–5	2–4
Mean hyphal width, μm	Mean width is used to derive a minimum area, to reject debris based on size	4–5	2–3
Minimum length, μm	Minimum length is used to derive a minimum area, to reject debris based on size	20–30	10–20
Number of loops	To re-classify mycelia into freely dispersed and clumps based on the number of loops. Loops are caused by simple overlapping of branches	3	3
Maximum fullness ratio	The value of the fullness ratio above which particles are classified as debris or large media particles	0.6–0.7	0.6–0.7
Circularity factor	Used to remove rounder media particles and debris	2–3	2–3

focus. The image was captured and stored in digital format. This grey image was enhanced by delineation. It was then detected to obtain a binary image. The binary image was then subject to a single closing operation to consolidate the detection. The subsequent major image processing stages are described diagrammatically below.

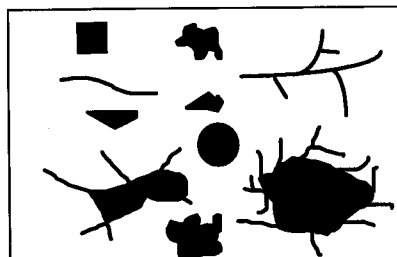
1. Diagrammatic representation of a binary image obtained after detection of a grey image followed by closing operation. The image might contain many small background artefacts and medium particles which were removed by a single opening operation.



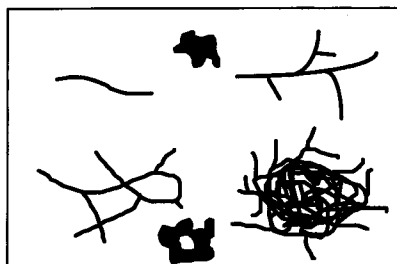
2. Most of the smaller non-hyphal particles not eliminated by the opening operation of step 1 were removed using a size (area) filter derived from the specified mean width and the minimum length parameters.



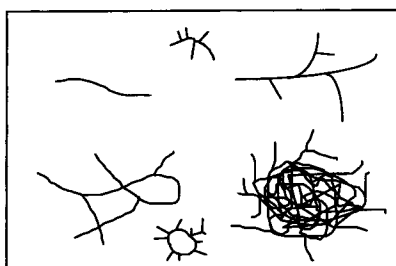
3. A binary filling operation was applied to fill the internal holes or voids of each object.



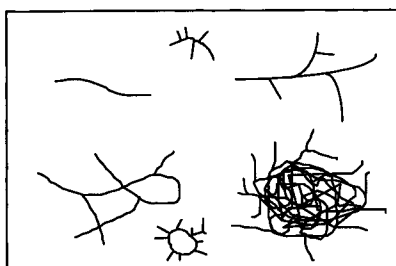
4. A circularity (shape) factor filter was applied to remove media particles and debris which appear more round than mycelial particles. Remaining objects were restored to their unfilled forms.



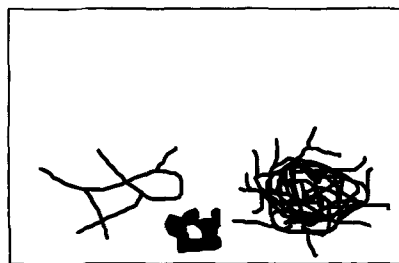
5. The image was skeletonised.



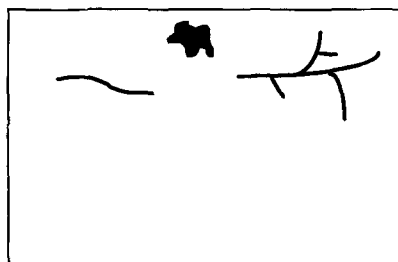
6. An exhaustive pruning was applied to the skeletonised image which removed all skeletons not containing a loop, i.e. unbranched and branched mycelia, and debris appearing as unholed.



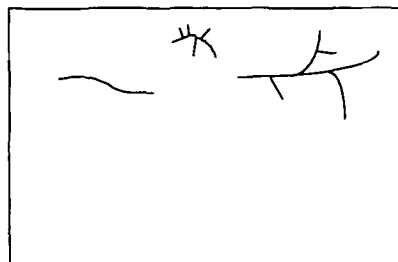
7. The loop-containing objects were then reconstructed from the image in step 4 using loops from step 6 as seeds.



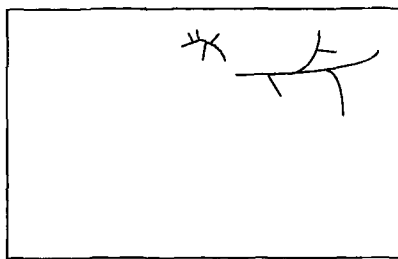
8. By subtraction of image 7 from image 4, an image containing unbranched and branched mycelia including some debris was obtained.



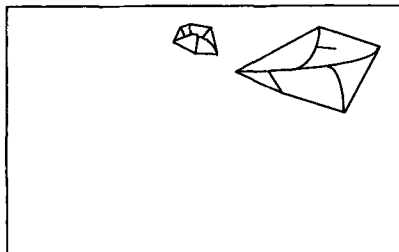
9. The image was then re-skeletonised.



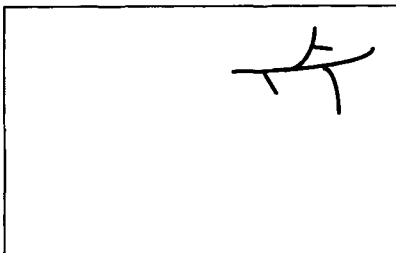
10. The unbranched hyphae were separated based on the number of branching points. Before this operation the skeletons were pruned to remove any false branches or small touching particles of lengths less than the minimum specified.



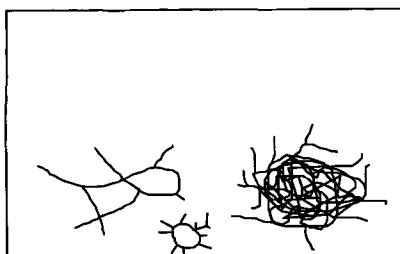
11. The outer points of the remaining objects were joined to give the convex perimeter of each object. A wrapping algorithm was used to find and join these outer points [29].



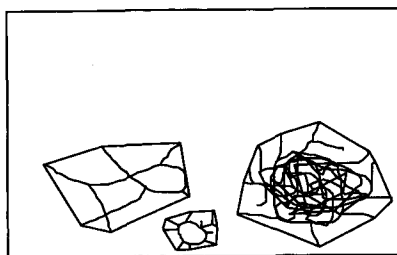
12. For each of the objects in image 11, the ratio of its actual area (step 8) to the convex area gave a fullness measurement for that object. Debris usually gave higher fullness ratios than branched mycelial particles, and could be eliminated on this basis.



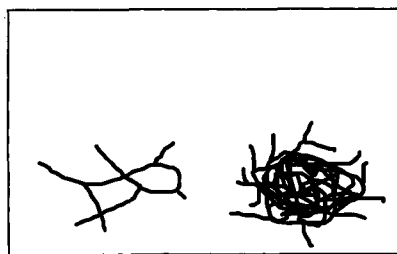
13. A skeletonised image of mycelial clumps and remaining debris, derived from the image of step 7.



14. The convex area of each object was obtained by applying the wrapping algorithm.



15. The non-hyphal particles were then eliminated using the fullness criterion. A further classification of clumps was based on the number of holes. A lesser number of holes usually indicates artefactual overlapping rather than a real clump. This latter class is termed as simple clumps or “entanglements” (MN Paris; personal communication) and are considered to be part of the class of freely dispersed mycelia.



Following the elimination of non-hyphal particles and classification of all the mycelial elements, measurements were performed. The image containing branched hyphae could be processed further to identify individual branches by branch order. The detailed description of image processing operations for this step can be found in a paper by Tucker et al. [13]. This optional measurement of individual branches is not usually done, in order to increase the speed of analysis. The hyphal measurement parameters are listed in Table 3. Information on each particle was stored in a file for detailed statistical analysis, e.g. mean and standard deviation calculations, and for generating histograms.

Figure 11 illustrates the different types of morphology of *S. clavuligerus* in a submerged batch fermentation obtained by using different inoculum spore concentrations [30]. In general, fungal species also show a similar range of morphological forms in submerged fermentations. Image analysis [3, 31, 32, 34] has recently been used to replace manual method [33] in studying the effect of the initial spore concentration, medium pH and medium composition on the growth and morphology of fungal fermentations. The developed morphology in the fermenter is also influenced by the agitation, which can lead to even more heterogeneous forms and sizes. Figure 12 shows the morphological parameters of the freely dispersed hyphae, i.e. unbranched and branched hyphae and entanglements (combined together), throughout a fed-batch penicillin fermentation in

Table 3. Hyphal morphology parameters obtained by image analysis (see Table 1 for definition of these parameters)

Mycelial classes	Parameters
Unbranched	Total length Mean width Area and area fraction
Branched	Total length Branch order and individual branch length Longest length Maximum dimension Number of tips Mean width Internodal distance Hyphal growth unit length Hyphal growth unit volume Area and area fraction
Simple clumps (containing 1–3 holes) or "entanglements"	Total length Maximum dimension Mean width Number of tips Internodal distance Hyphal growth unit length Hyphal growth unit volume Roughness Fullness ratio Area and area fraction
Clumps	Maximum dimension Roughness Fullness ratio Area and area fraction

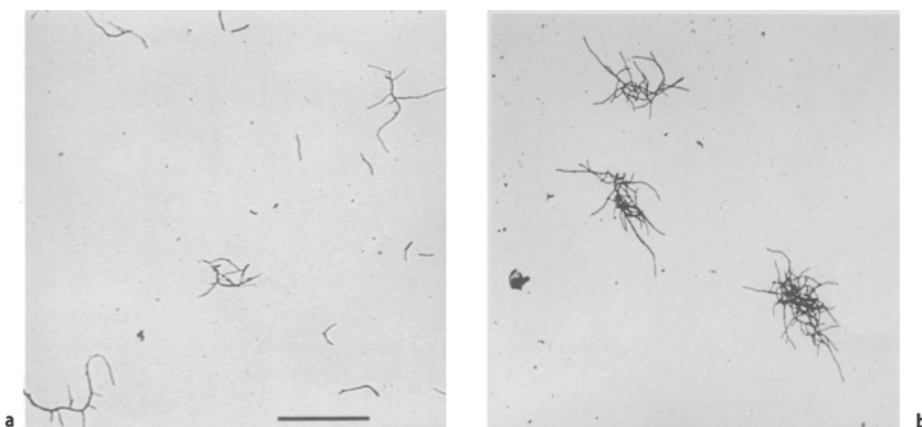


Fig. 11 a, b. Different classes of morphology from a submerged *S. clavuligerus* fermentation: a freely dispersed mycelia; b small clumps; c bigger clumps; d a pellet (bar length = 60 µm)

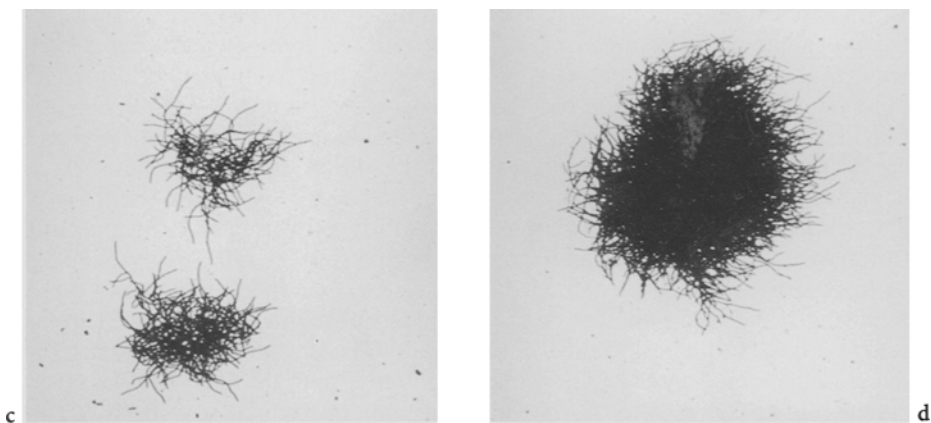


Fig. 11 c, d

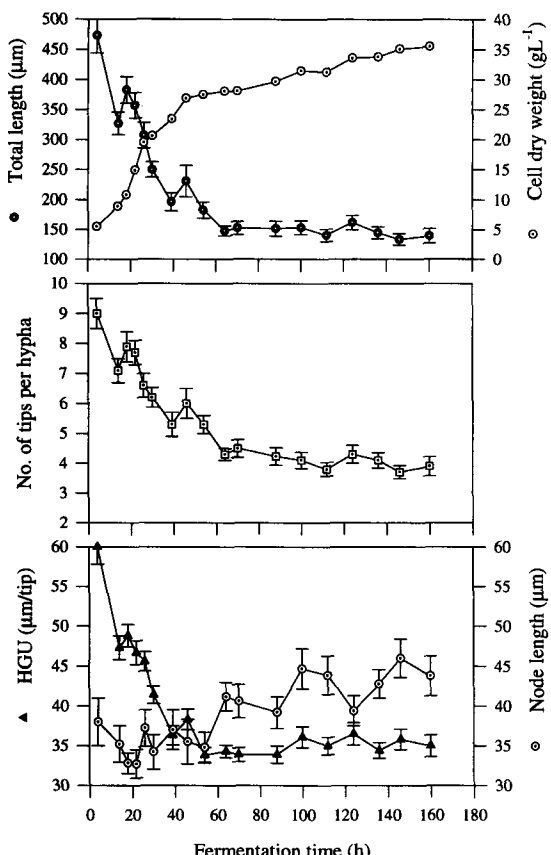


Fig. 12. Time profiles of cell dry weight and the mean values of total length, tips per mycelium, hyphal growth unit and node length for freely dispersed hyphae from a typical fed-batch *P. chrysogenum* fermentation with constant glucose feed rate

which nutrient concentrations change with time. Figure 13 shows the corresponding morphological parameters for the clumps. The fermenter was inoculated with 32 h-old vegetative inoculum containing mainly freely dispersed mycelia grown on a complex medium in a shake flask. As can be seen in Fig. 13, the proportions of clumps by projected area, the mean clump fullness and the mean clump maximum dimension increased during the rapid growth phase which ended approximately 24 h after inoculation. During this period, the mean total length and the mean number of tips per hypha dropped significantly, possibly due to fragmentation of the inoculum mycelia which were significantly vacuolated before transfer to the fermenter. After 24 h, there was a rather rapid drop of mean total length and mean number of tips per hyphae. Fragmentation of the clumps was also observed as can be seen from Fig. 13. The proportions of clumps, the mean fullness ratio and the mean maximum dimension declined and the mean clump roughness rose. All of these changes after 24 h might have been due to increased vacuolation of the hyphae (see Sect. 3.4) as the carbon source became

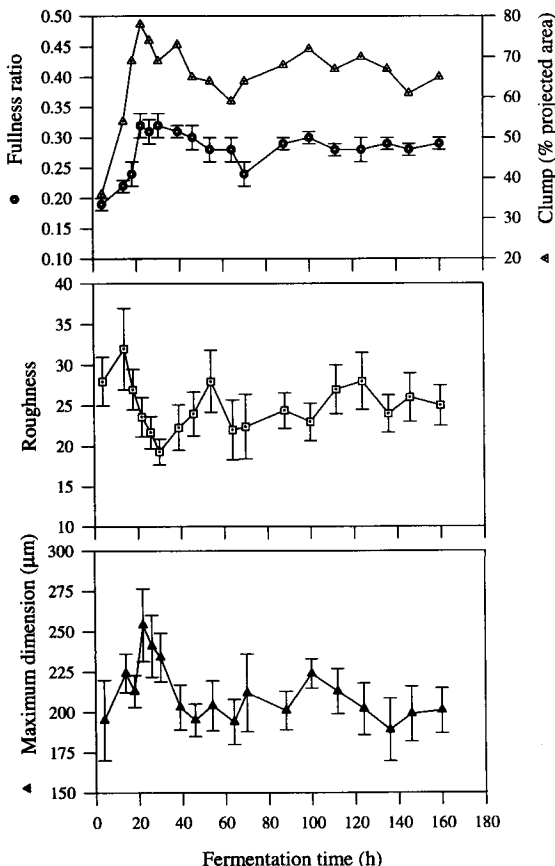


Fig. 13. Time profiles of the proportion of clumps and mean values of fullness ratio, roughness and maximum dimension for the fed-batch *P. chrysogenum* fermentation shown in Fig. 12

depleted at the end of the rapid growth phase [35]. It must be noted however that the apparent reduction of the hyphal lengths for the freely dispersed mycelia might be due, at least in part, to loss of fragments from clumps, fragments which reappear in the freely dispersed category affecting its size distributions. This needs further study.

For most industrial mycelial fermentations, dispersed growth is preferred and for such fermentations image analysis can have an important role in characterising morphology. It should be noted here that a high degree of clump formation in submerged fermentations implies that classical morphological measurements on the freely dispersed class alone provide only partial information which is based on only a small fraction of the total biomass. There is little point in making measurements on only the freely dispersed form, especially as evidence exists that the hyphal elements within clumps are of different morphology to those not aggregated [36]. Fully automatic characterisation of morphology including clumps is now possible, which opens up new research opportunities in engineering and physiological studies of mycelial fermentations.

Modelling mycelial morphological development is very complex. Nevertheless there are several models available in the literature concerning hyphal growth and branch formation [37–41]. Chapter 4 gives a general review of morphological models of *Penicillium* species and Chap. 3 of *Streptomyces* species. Modelling in submerged fermentations still involves many unproven assumptions because of the complex interactions of fermentation environments and mycelial morphology and because of lack of knowledge, particularly of the kinetics of the formation and breakage of clumps in real fermenters. For this purpose fully automatic image analysis can be used to gather the large amounts of data needed for model development, extension and verification.

3.2

Pellet Morphology

There are a number of image analysis methods available to characterise pellets from submerged fermentations. Reichl et al. [42] used image analysis to study *S. tendae* pellets, measuring for each sample the frequency distribution of size, the mean size, the percentage of total mycelia (by projected area) that existed as pellets, and pellet shape. Pellets were distinguished from hyphal fragments and clumps by greyness level differences; they were relatively dark. This approach provides a possible definition of a pellet. The pellet-shape analysis relied on image-processing operations which affected the irregular outline of fluffy pellets more than that of smooth ones. The shape factor thus obtained was the first proposed for quantitative discrimination between pellet types. Durant et al. [43] discriminated between these zones by rinsing out a stain (i.e. by a diffusional criterion) which made image analysis much easier. Later, the method was improved using colour-image processing [44].

Pichon et al. [45] and Cox and Thomas [14] proposed image analysis methods to characterise pellets based on the presence of a central core. Each pellet was analysed using grey image processing giving darker regions in the pellet-centre

and relatively brighter outer mycelial regions. Cox and Thomas [14] further classified the pellets into smooth and hairy types using automatic image analysis. The central core was identified by removing the lateral hyphae by image processing. The core size (projected area) and shape (circularity) were determined. The hairy annular region of lateral hyphae was also characterised in terms of size, fullness and roughness. The method was developed on the Quantimet 570 using simple image processing operations common to most commercial image analysis software packages and can therefore be implemented easily on other systems. This method is described here in a greater detail.

3.2.1

Sample and Slide Preparation

Samples from *A. niger* fermentations were fixed in an equal volume of fixative containing 9% (w/v) formaldehyde and 50% ethanol. The pellets and mycelia were stained with lactophenol cotton blue to enhance visualisation under bright field illumination. The three dimensional structure of the pellets was preserved by observing pellets in a cavity slide of depth 1 mm. The typical analysis time for a pellet is approximately 5 s [14], so that a few hundred pellets can usually be characterised in 15 min.

3.2.2

Image Analysis Parameters

Table 4 gives the list of image analysis parameters and their typical values used for *A. niger* pellet analysis.

3.2.3

Image Analysis Software

Pellets of sizes less than 600 µm equivalent diameter were viewed under a microscope (as described in Sect 3.1). For larger pellets a macroviewer was used. This consisted of a CCD camera fitted with a macroscopic zoom lens mounted on an adjustable camera stand allowing transmitted light examination of samples. Movement of the sample in the field of view was manual.

Table 4. List of image analysis parameters and their typical values

Parameter	Use	Typical range (cycles)
Erosion	To remove smaller non-hyphal debris and media particles	3–6
Opening	To remove lateral hyphae to find the pellet core	4–6

An image of pellets was acquired and delineated to increase the outline definition. The image was then detected to produce a binary mask of the pellets overlaying the grey image. The subsequent image analysis was on this binary image. Small debris and media particles including small mycelial fragments were first removed from the image by repeated erosion until they vanished, leaving the pellets and mycelial clumps, which are larger, not completely eroded away. A rebuilding operation (based on the original binary image) was then used to restore pellets and mycelial clumps to their original size. The analysis of any individual pellet involved the recognition of the solid core within it. The existence of a core was ascertained by an ultimate skeletonisation of the pellet image, i.e. the exhaustive removal of the outer pixel layers of the skeletonised image to identify a central single pixel marker. However, the presence of holes in the annular regions created by entangled lateral hyphae prevented this marker being located by reducing down to loops rather than a single point. If this occurred, lateral entangled branches were removed by an opening operation. Repeated opening cycles were done until an ultimate skeletonisation did give a single marker, or until the preset maximum number of openings was reached (Fig. 14). Once a marker was identified, the pellet was rebuilt from it. The pellet was then subjected to an opening operation to remove the annular hyphal region and separate out the core. The subtraction of the core from the whole pellet gave the annular regions. An object without a core identifiable with the preset maximum number of openings was

Image processing steps	After ultimate skeletonisation
Original image	
After one- cycle opening	
After two- cycle opening	
After three- cycle opening	
	•

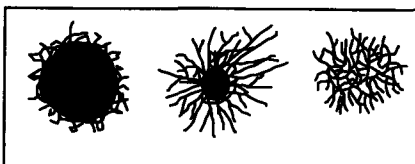
Fig. 14. Image processing operations to identify the core of a pellet. In the illustrated case, after three cycles of opening skeletonisation gives a single pixel marker. The core has then been identified

classified as a clump. Figure 15a–c shows different forms of morphology and their classification on the basis of structure.

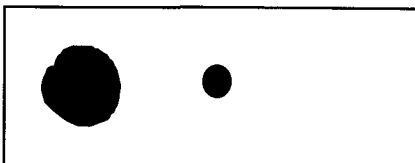
Figure 16 shows a smooth and a hairy pellet of *A. niger* from a submerged citric acid fermentation. Figure 17a shows the biomass growth, mean pellet equivalent diameter and mean core equivalent diameter across the time course of an *A. niger* batch fermentation. Both the whole pellet diameter and the core diameter increased with time and followed the growth of biomass in the fermenter. After 50 h, the annular regions grew faster than the core. Figure 17b shows the mean projected area of the cores and the mean core circularity. More regular core shapes were found later in the fermentation. Figure 17 c gives the corresponding mean annular area and the mean whole pellet fullness ratio. The coincidence of the increase of annular area and the decrease of fullness suggests that growth of the annular regions took place by the extension of hyphae in these regions, therefore increasing the hairiness of the pellet. This can be seen more clearly from Fig. 17d from the mean ratio of convex area of a core to that of the whole pellet. This suggests that there existed a transition of morphologies from smooth to hairy after 50 h in this fermentation.

Pellets of some strains are sensitive to agitation conditions. At high agitation levels pellets can be fragmented. Figure 18 shows the time profiles of mean pellet

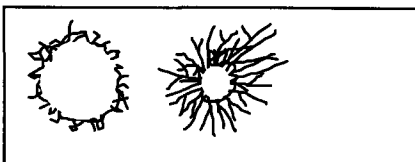
- a) An image containing a smooth pellet, a hairy pellet and a mycelial clump



- b) Pellet cores



- c) Pellet annular regions



- d) Mycelial clump classified as an object without the presence of solid core

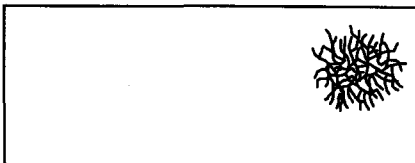


Fig. 15. Diagrammatic representation of the classification and characterisation of pellets

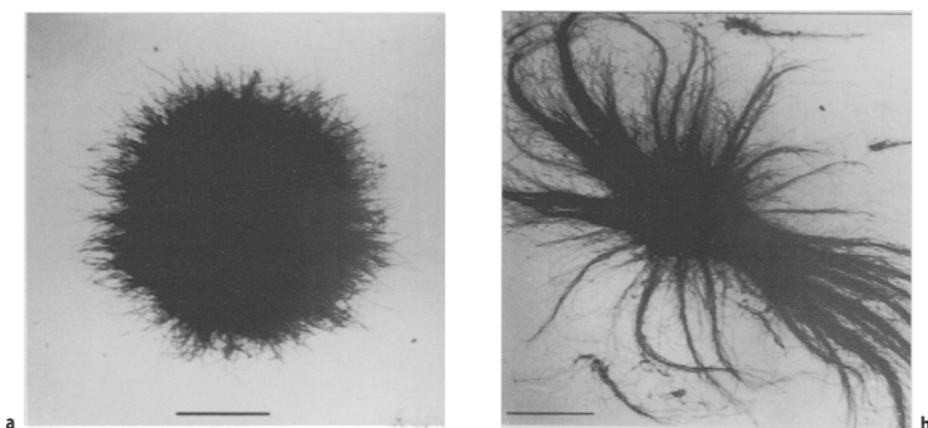


Fig. 16 a, b. *A. niger* pellets from a submerged citric acid fermentation: a smooth pellet; b hairy pellet (bar length = 0.25 mm)

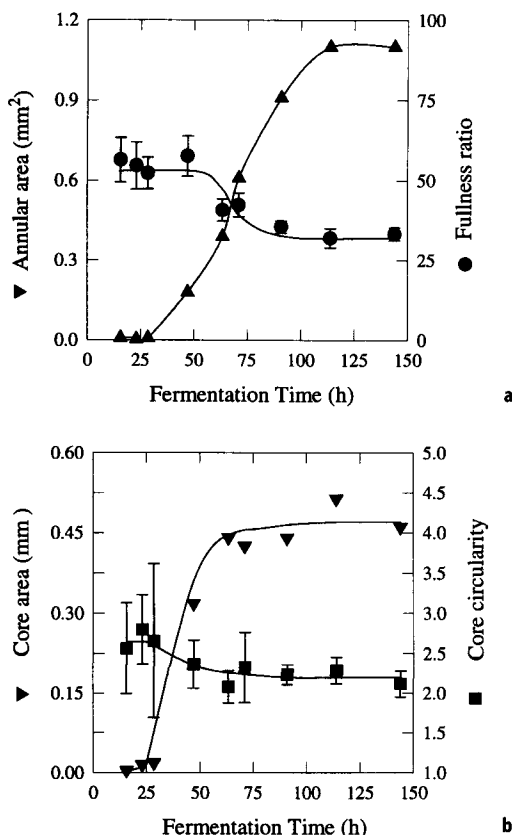


Fig. 17 a, b. Pellet growth characteristics in *A. niger* batch culture: a cell dry weight and the mean equivalent diameter of the whole pellet and core; b mean core area and mean core circularity

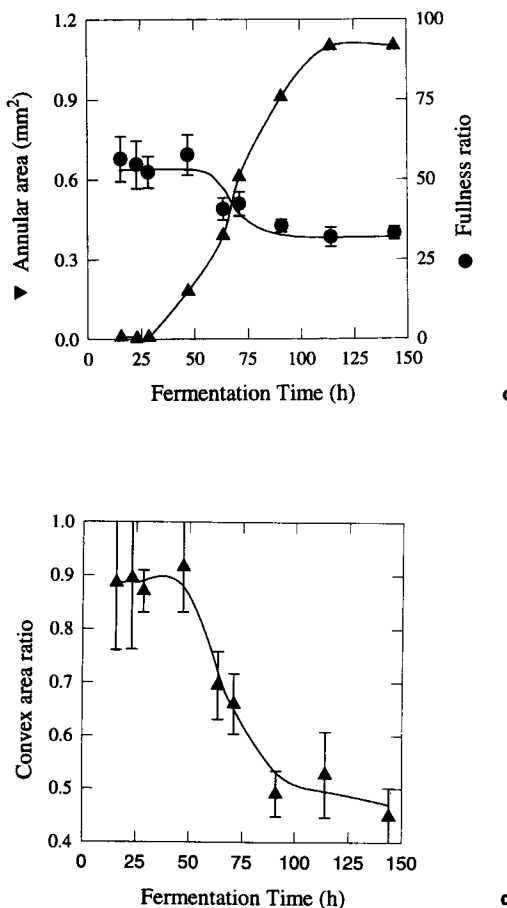


Fig. 17 c, d. c mean annular area and mean annular fullness; d ratio of mean convex area of core to mean convex area of the whole pellet [14]

equivalent diameter and mean core circularity of an industrial strain of *A. niger* grown at 5-l fermenter scale [3]. With a low agitation speed (300 rpm) the pellets of initial mean equivalent diameter 1.4 mm grew larger with fermentation time until they were of mean diameter 3.2 mm at 96 h. Then the agitation was increased to a very high level of 800 rpm and the pellets fragmented rapidly to 1.6 mm mean diameter. The fragmentation of pellets was associated with an increase of metabolic activity as can be seen from the carbon dioxide production rate (CPR) and oxygen uptake rate (OUR) data presented in Fig. 19. Edelstein and Hader [46] and Tough et al. [47] developed population balance models for pellet growth and fragmentation in submerged fermentations. Chapter 3 describes a review of the modelling of pellet growth and fragmentation of *Streptomyces* spp.

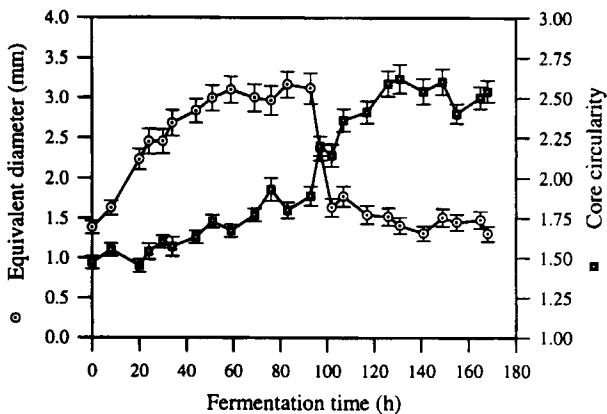


Fig. 18. Effect of agitation speed on the fragmentation of *A. niger* pellets. Agitation speed: 300 rpm from 0 to 12 h, 500 rpm 12 to 96 h, 800 rpm 96 to 168 h

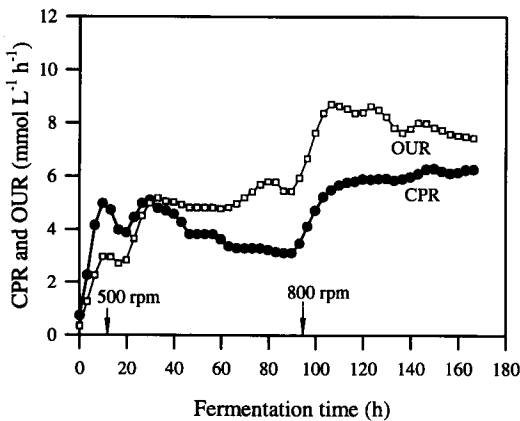


Fig. 19. The metabolic activity in the fermentation of Fig. 18 is influenced by pellet breakup following the increase of agitation speed

3.3

Fungal Spore Germination

An automatic image analysis method was developed by Paul et al. [15] to study the viability and germination characteristics of fungal spores for samples from submerged inoculum cultures. This was intended to replace the traditional plate count technique in which a dilute suspension of spore is spread on a solid agar medium and the fractional spore viability is assessed by counting the isolated colonies. Because the germination of spores depends on the composition of the medium as well as on the growth conditions the information obtained from a plate count cannot be applied directly to submerged culture. The image analysis method works on samples taken from the fermenter or shake flask, so the spores

can be under appropriate conditions. In addition to fractional germination, the image analysis method also gives spore swelling characteristics and the germ tube formation and extension kinetics. These are potentially valuable in studies of the quality of initial spore preparations and proposed inoculum media.

3.3.1

Sample and Slide Preparation

Exactly 1 ml of each sample of *P. chrysogenum* spores from the inoculum fermenter or shake flask was fixed with 3–4 drops of lactophenol cotton blue stain (Fluka). A sample could be stored for up to 7 days at room temperature. A Helber counting chamber (Weber Scientific Int., Middlesex, UK) with a depth of 20 µm was used to estimate the spore concentrations along with other germination parameters. The chambers were supplied without grid lines to ease the image processing. When germination was significant, the culture was diluted with an equal volume of distilled water to separate objects on the slide before analysis. Approximately 0.04 ml of the (diluted) culture was placed on the counting surface. The chamber was closed with a thick optically flat coverslip.

3.3.2

Image Analysis Parameters

Image analysis parameters for this application and their typical values for a *P. chrysogenum* fermentation are listed in Table 5. These were set using samples from a preliminary germination experiment and could then be used for other experiments with the same organism and medium. Settings for the lower limit of diameter and for the maximum circularity depend on the type of spores in use and could be obtained from a preliminary experiment on unswollen spores. To discriminate between non-germinated spores attached to some other spore and a genuine germ tube, the minimum circularity for germ tubes was set equal to the maximum for unswollen spores. The parameter for the lower limit of germ tube length was set to eliminate artefacts caused by small debris touching the spores.

The four parameter values described above could be kept constant throughout a germination test on *P. chrysogenum* spores. The other two parameters were

Table 5. Image analysis parameters and their typical values used for the image analysis of *P. chrysogenum* spore germination

Parameters	Typical values	Values preferable at early stages	Values preferable at late stages
Minimum spore diameter, µm	2–3	2–3	2–3
Maximum spore diameter, µm	5–16	5–8	5–16
Minimum germ tube length, µm	2–3	2–3	2–3
Maximum germ tube length, µm	10–50	10–20	10–50
Circularity limit for spores	≤ 1.2	≤ 1.2	≤ 1.2
Circularity limit for germ tubes	> 1.2	> 1.2	> 1.2

settings for the maximum spore diameter and the maximum length of a germ tube. These parameters are used to distinguish between spores, germ tubes and debris. It was found that the accuracy of the measurements could be improved if different values of these parameters were used in the early and late stages of germination (Table 5). This was particularly important when large amounts of debris and media particles were present.

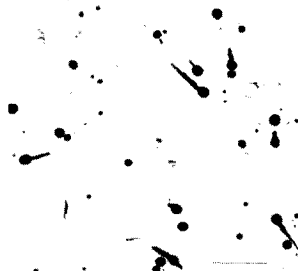
The magnification used for *P. chrysogenum* spores was $\times 200$. The typical number of spores (non-germinated + germinated) per sample was 400. The total number of fields for analysis of this number of spores was in the range of 25 to 32, 17 to 13 spores per field respectively. The time of analysis for this number of spores varied between 10 and 22 min depending on the complexity of the samples and number of spores per field of view.

3.3.3

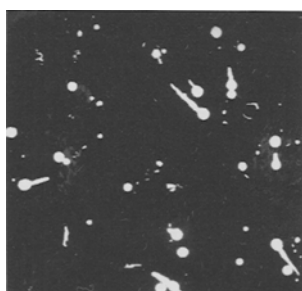
Image Analysis Software

An image of spores is captured from a microscope field of view and then stored. The image is then detected and all the image processing operations are done on the detected binary image.

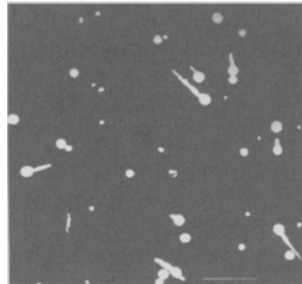
1. A typical captured image of *P. chrysogenum* spores 16 h after inoculation in a defined medium. The image contains both non-germinated and germinated spores. It also contains many undesired objects and debris (particularly dead mycelia) and small particles.



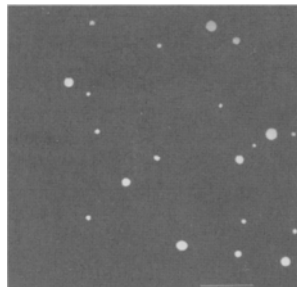
2. The image after detection of the original grey image. The subsequent image processing operations were on this binary image.



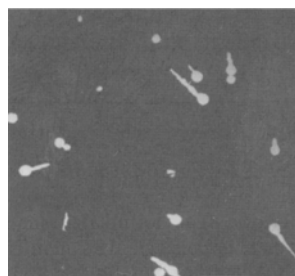
3. The binary image was subjected to a two-step erosion operation which removed most of the small particles. The image was then rebuilt to its original form, excluding those small extraneous objects. The larger unwanted objects could be identified by using a larger erosion (10–16 steps) which removed spores and similar sized debris, leaving only the cores of the large debris. After rebuilding the latter to its original size, it could be subtracted from the earlier image, leaving a new image which contains spores and germ tubes and some spore-sized debris.



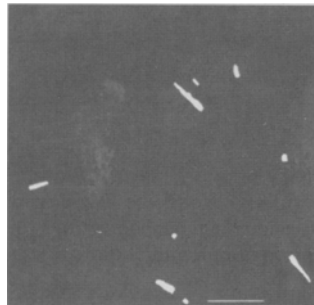
4. Objects in image shown above were then classified into two groups using a preset circularity parameter. The objects in this image are definitely non-germinated spores obtained by setting circularity ≤ 1.2 .



5. Objects in this image were obtained by subtraction of the image in step 4 from that in step 3. This is equivalent to applying circularity > 1.2 to objects in image 3. This image contains germinating spores, non-germinated spores artefactually attached to germ tubes of other spores, touching non-germinated spores, and non-germinated spores touching one of those germinating, as well as debris.



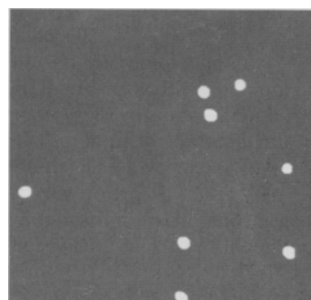
6. The germ tubes and the touching objects were then separated by a multistage opening operation. The opening removes the narrow touching objects including the germ tubes, leaving behind the wider germ tube spores. By this process objects (mostly debris) without a spore were eliminated. Subtraction of the germ tube spores from those shown in step 5 gave germ tubes and touching non-germinated spores. Germ tubes were identified using preset circularity and size criteria and are shown in image 6.



7. The germ tubes of the germinated spores identified by the procedure described above and then superimposed with the image in step 5 to identify the germinated spores.



8. The germ tube spores of the germinated spores were identified by using the germ tubes as markers. The spores connected with the germ tubes are presented in this image.



9. The touching or connected objects classified as nongerm tubes in step 6 were reclassified to non-germinated spores using a preset circularity parameter. These extra non-germinated spores were finally added to those obtained previously shown in step 4. This image contains all the non-germinated spores.

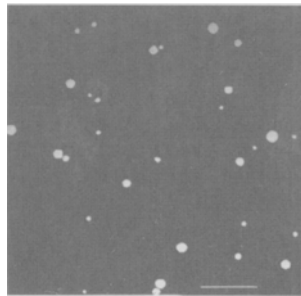


Table 6. Lists of parameters obtained from the measurement and calculation of spore samples from inoculum cultures

Classification	Parameters
Non-germinated spores	Total number Number fraction Concentration Equivalent diameter Circularity Area Volume
Germ tube spores	Total number Number fraction (fractional germination) Concentration Equivalent diameter Circularity Area Volume
Germ tubes	Total number Length Mean width Area Volume

3.3.4

Measurement

Measurements were performed on images shown in steps 9, 8 and 6 representing the non-germinated spores, germ tube spores and germ tubes respectively. Table 6 lists the parameters obtained from image measurement.

The method was tested using three media and two spore stocks of *P. chrysogenum*, one collected after 6–8 days of incubation at 25 °C while the other was

obtained from a 40-day old culture stored at 4 °C after 6–8 days in the incubator at 25 °C. Table 7 lists the inoculum experiments [15] using different media and two spore ages. Figure 20 shows spores for samples taken at 20 h from shake flasks containing defined medium M2. The spores in Fig. 20a were grown from stock S1, whereas those of Fig. 20b were grown from stock S2. It is clear that the latter did not germinate as well as the former, indicating that the germinability of the spores deteriorated with the duration of storage. Figure 21 shows the percentage of germinated spores against incubation time in the three different media and with two ages of spores. These very different spore preparations combined with the range of media used gave an excellent test of the image analysis method.

The proportions of the spores which formed germ tubes and the time of germ tube formation were affected by medium and spore age. At 24 h, 89% of the spores had germinated in the complex medium M4, compared to only 16% in

Table 7. List of inoculum experiments using *P. chrysogenum*

Experiment	Medium	Spore type
S1M1	Defined medium [48].	Fresh spores (S1)
S1M2	Medium M1 with double the Fe ⁺⁺ salt and supplemented with 0.6 g l ⁻¹ Na-EDTA.	Fresh spores (S1)
S1M3	Complex medium [49].	Fresh spores (S1)
S1M4	Solids of M3 removed and supplemented with 1.0 g l ⁻¹ Na-EDTA.	Fresh spores (S1)
S2M2	Medium M2.	Old spores (S2)
S2M4	Medium M4.	Old spores (S2)

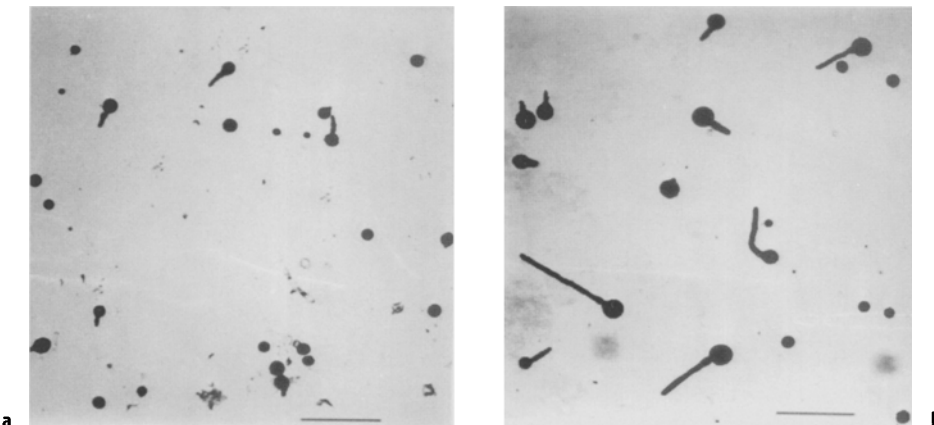


Fig. 20 a, b. *P. chrysogenum* spores taken at 20 h in medium M2 with spore stock: a S1; b S2. Photographs were taken from the image analyser display. Bar length = 50 µm [15]

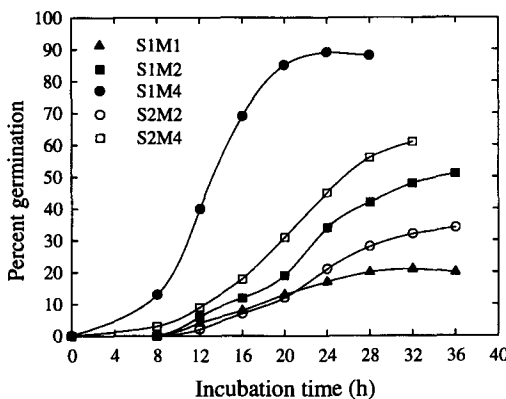


Fig. 21. Time course of germination of *P. chrysogenum* spores in different inoculum media and two ages of spores [15]

the defined medium M1. When the concentration of Fe^{++} in M1 was increased twofold (to give medium M2), the germination level increased from 16 to 33 %. The defined media M1 and M2 required longer incubation times for germination than the complex medium. It can also be seen that germinability of spores deteriorated significantly with storage. The 40-day old spore (stock S2) had only germinated 21 and 45 % in media M2 and M4, respectively after 24 h, compared to 33 and 89 % germination with fresh spores (stock S1). Nielson and Krabben [39] used this image analysis information to fit their 5 parameter β -distribution model (see Chap. 4).

The mean volumes of non-germinated and germ tube spores during the course of the incubation are presented in Figs. 22 and 23, respectively. Spherical growth of the spores progressed with continuing incubation. The media had a marked influence on spore swelling and their eventual size, with higher swelling

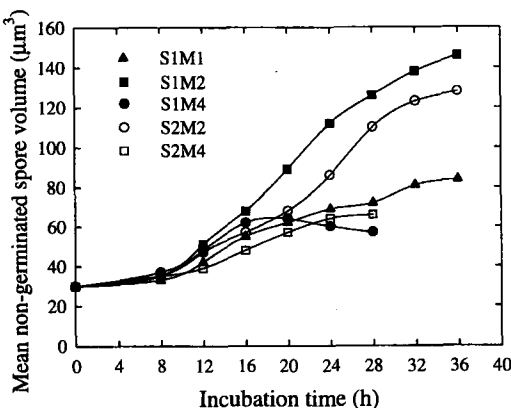


Fig. 22. Time course of mean volumes of non-germinated spores of *P. chrysogenum* in different inoculum media and using two ages of spores [15]

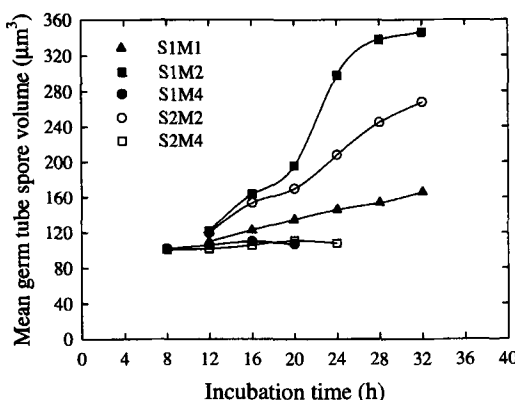


Fig. 23. Time course of mean volumes of germ tube spores of *P. chrysogenum* in different germination media and using two ages of spores [15]

in the defined media. It can be seen in this plot how the mean size of the non-germinated spores in the complex medium M4 was restricted by rapid germination which removed spores into the germinated class early in the swelling process. The mean volume of spores alone might not be adequate to represent the swelling process, as each sample contains a wide range of spore sizes, whether germinated or not. Image analysis can also provide the distributions of spore sizes as shown in Fig. 24 for defined medium M2. Together with percent germination and the spore size distribution a population balance model was proposed by Paul and Thomas [50] to describe the inoculum stage of fungal fermentations. However, such modelling is still not entirely satisfactory because the information on the physiology of spore germination that would pull together the relationship between spore swelling and germ tube emergence is not available.

Besides spore characteristics, germ tube lengths of the germinating spores could also be found by image analysis (Table 6). Figure 25 shows the mean length of the germ tubes during the course of incubation in different media with both spore stocks (S1 and S2). Mean germ tube length increased with incubation time. Differences of germ tube growth with different medium and spore ages are evident in this figure.

The method described here offers a number of advantages over photomicroscopy or colony counting (on solid media) to determine spore viability: it is rapid, is more accurate and consistent, can discriminate between non-germinated and just germinated spores, and in particular can be used on spores germinating in the actual submerged fermentation medium under appropriate agitation and aeration conditions. It provides measurements on spore preparations that are very appropriate for assessment of the quality of an inoculum. This method might be used to study the effects of medium formulation on germination and for the development of better inoculation methods as part of the optimisation of fungal fermentations. For complete studies of early hyphal extension and branching phenomena this method might be used in conjunction with that of Tucker et al. [13].

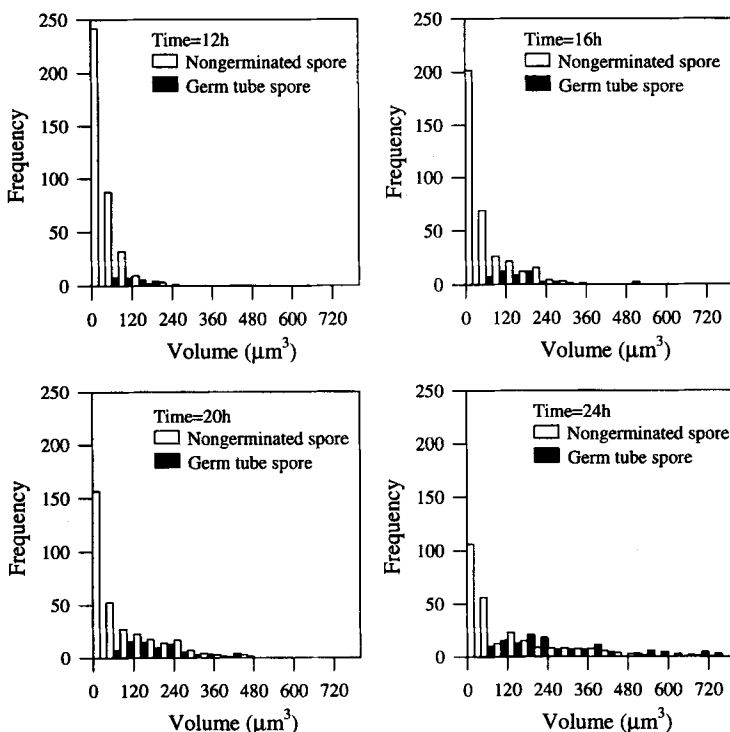


Fig. 24. Comparison of distributions of non-germinated spore and germ tube spore volumes of *P. chrysogenum* grown in medium M2 using spore S1 [15]

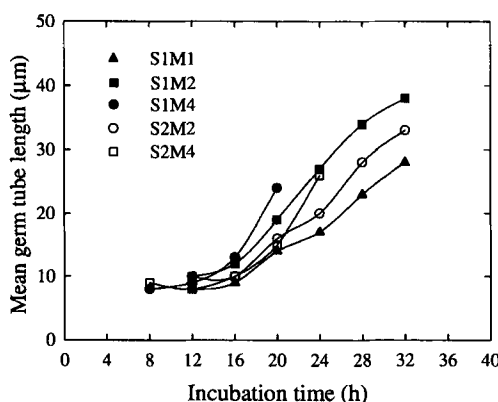


Fig. 25. Time course of mean volumes of germ tube lengths of *P. chrysogenum* in different germination media and using two ages of spores [15]

3.4

Hypal Differentiation

For the filamentous form of fungi, differentiation of the hyphae may be characterised by image analysis. Packer et al. [51] identified two different regions of *P. chrysogenum*: (1) the cytoplasmic regions, and (2) degenerated regions including large vacuoles. The volume occupied by each of these regions in a fixed volume of sample could be estimated and hypal-density values for each region could be used to estimate biomass concentrations from 0.03 to 38 g/l, even in the presence of up to 30 g/l of the solid ingredients often found in commercial media. This method gives some information needed to build a structured model such as that proposed by Nestaas and Wang [52]. It was, however, rather slow (several hours per sample), although no attempts were made to speed up the process.

Paul et al. [7] have developed a new image analysis method for a detailed characterisation of fungal vacuoles in terms of the percentage by volume of vacuoles and empty regions, and vacuole size and shape. Figure 26 shows by images how vacuoles can be identified by this method, which involves very complicated image processing operations reported in detail in Paul et al. [27]. Recently the method has been extended to identify and quantify the proportion of growing regions [8]. This section describes this image analysis method for complete characterisation of simple differentiation, i.e. growing regions (mainly apical), non-growing regions, vacuoles, and empty regions.

3.4.1

Sample and Slide Preparation

Samples from fermentations were diluted with 20% (w/v) sucrose solution in order to prevent evaporation from the slide during image analysis. Final bio-

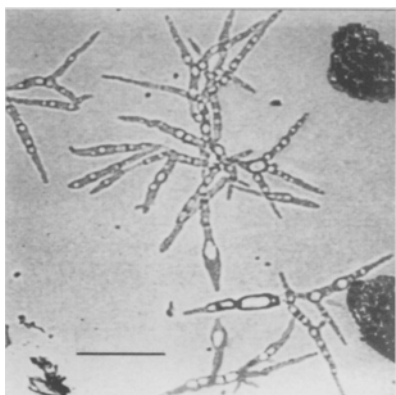
**a****b**

Fig. 26 a, b. Image analysis was used to characterise fungal vacuoles. a an original grey image; b a binary image of vacuoles and empty regions obtained after image processing operations [27]. (Bar length = 50 µm)

mass concentrations after dilution were 1 to 1.5 g/l. The pH of the diluted sample was adjusted to < 5.0 by the addition of dilute sulphuric acid. Approximately 0.1 ml of neutral red solution (BDH Ltd, Poole, UK) was added to 1 ml of the diluted sample. After 3–5 min a drop was pipetted onto a slide and covered by a cover slip. Analysis was done within 30 mins.

3.4.2

Setting Up of Image Analysis Parameters

The image analysis parameters used in the various filters described later and the typical range of their values are listed in Table 8. Usually a same set of values were used throughout analysis. With solid-containing complex medium a different set of values might be needed, particularly in the early stage of a fermentation when large quantities of solids might interfere with sample analysis.

3.4.3

Image Analysis Software

For each field of view to be analysed, a grey image was captured. Figure 27a shows a typical grey image of *P. chrysogenum* mycelia at $\times 200$ magnification, stored by the image analyser in the digitised form. The growing regions (stained apices) are darker than the remaining cytoplasm and vacuoles, whereas the greyness of vacuoles is lighter than cytoplasm and growing regions. The image was delineated to remove the intermediate greyness levels from the boundaries of the objects, resulting in sharpening of greyness gradients in those regions (see Sect. 2.2 for the delineation operation). Objects of interest in the delineated image were detected by greyness level. Two detection levels (chosen during setting up of hardware parameters) were used: a detection level for hyphae, i.e.

Table 8. Image analysis parameters and their typical range of values

Filter	Parameter	Value/limit
HYP1	Circularity	$C > 2.0$
	Closing	1
HYP2	Circularity	$1.0 \leq C < 3.0$
	Opening	8–12
	Area (μm^2)	$A \leq 25$
VAC	Circularity	$C > 2.0$
	Erosion	6–8
	Area (μm^2)	$3.1 \leq A < 78.5$
HYPV	Erosion	4–6
TIP	Area (μm^2)	$A > 20.0$
	Greyness	$G < 90$

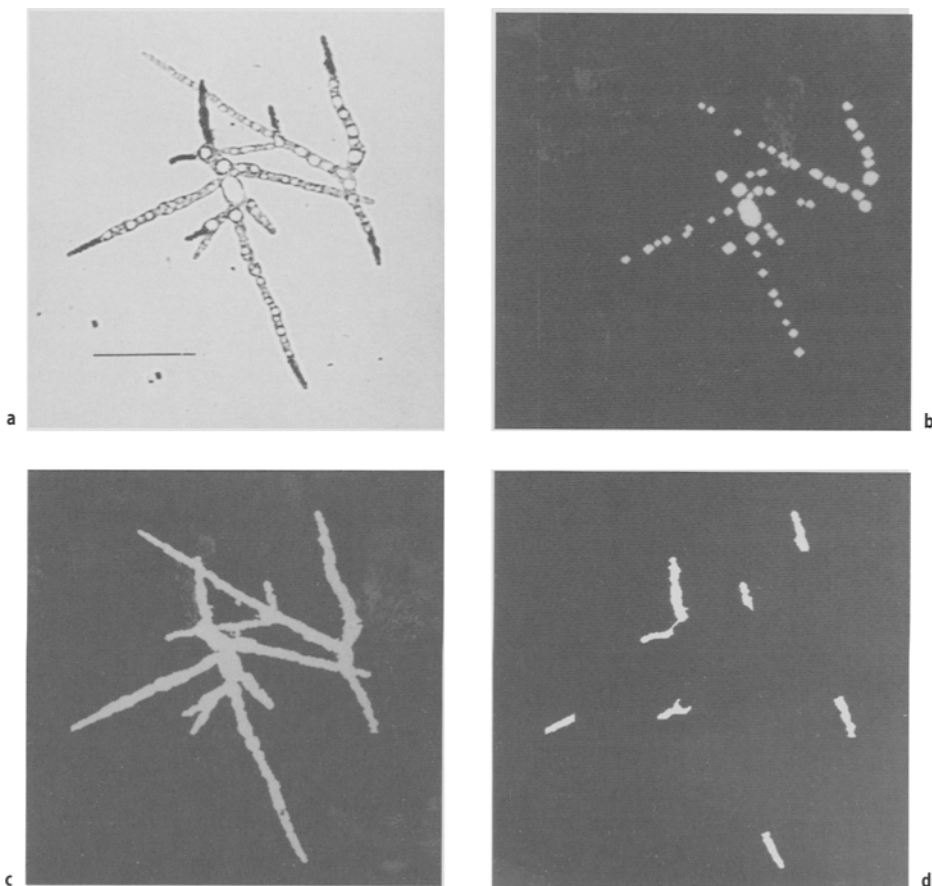
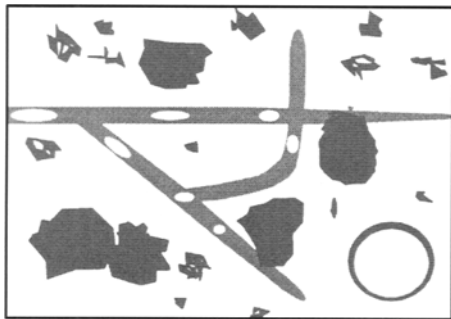


Fig. 27 a-d. *P. chrysogenum* mycelia at different image processing steps (bar length = 50 μm): a captured grey image; b binary image of vacuoles and empty regions; c binary image of hyphae including vacuoles and empty regions; d binary image of growing regions in the hyphae. The mycelia were from a typical fed-batch fermentation sampled during the production phase [8]

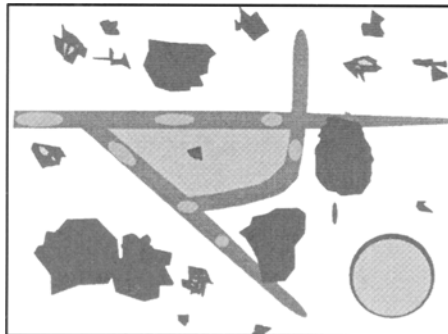
cytoplasmic regions and one for vacuoles and empty regions. These two binary images are referred to here as Image 1 (cytoplasmic regions) and Image 2 (vacuoles and empty regions) respectively. The microscopic images are not uniform in greyness which poses difficulties in separating features. The overall image processing steps were divided into three phases: Phase I consisted of elimination of debris, media particles and image artefacts; Phase II identification and separation of vacuoles and empty regions; and Phase III identification and separation of growing regions. Phases I and II are described using constructed images to illustrate the various stages of image processings involved and phase III using an actual image of *P. chrysogenum* hyphae.

Phase I.**Elimination of debris, media particles and other artefacts**

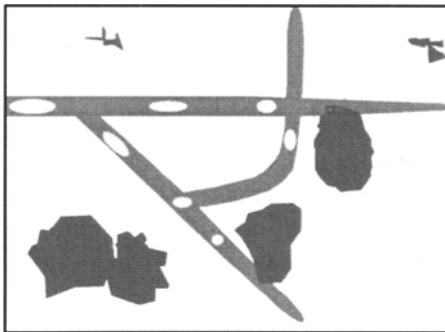
1. A diagrammatic representation of Image 1 (of hyphae excluding vacuoles and empty regions). Filter HYP1 was used on this image to correct small image imperfections, mainly pixels missing from the binary image because of the non-uniform intensity of the grey image. A closing operation was applied first to fill in the pixels missing due to poor detection.



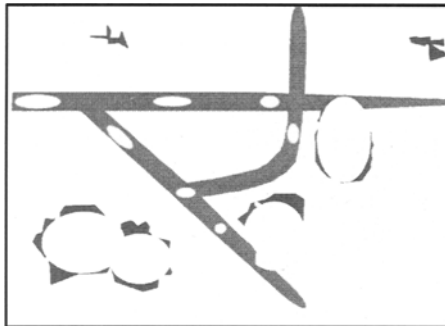
2. The consolidated binary image contained many non-hyphal objects and artefacts as illustrated diagrammatically here. These undesirable objects were identified and eliminated by the use of filter HYP2. An image filling operation was applied first by which internal voids or holes in an object could be filled.



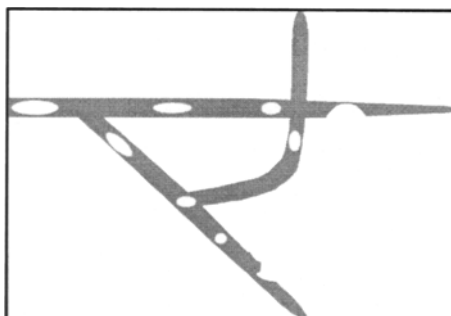
3. Most of the unwanted objects were identified as more circular than hyphae. This did not work on non-hyphal objects attached to hyphae because connected objects are processed as a whole.



4. The attached non-hyphal objects were identified for elimination by a number (preset) of opening operations. This removed the filamentous hyphae whilst leaving the wider non-hyphal objects. Subtraction of the non-hyphal objects from the original gave the hyphae and remaining small artefacts.

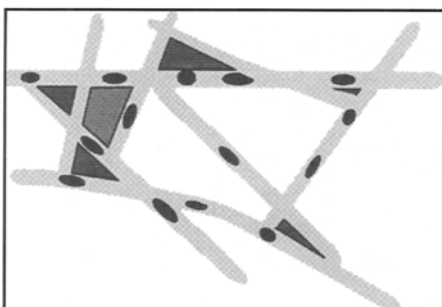
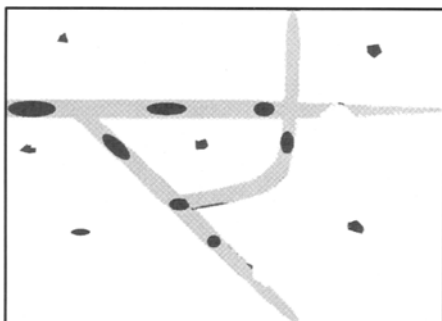


5. The smaller artefacts outside the hyphae created by the opening operation in step 4 were removed by the use of a preset size (area) filter.

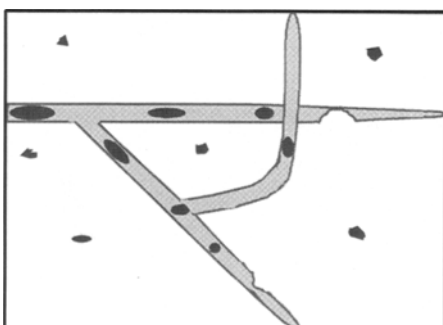


Phase II.**Identification and separation of vacuoles and empty regions**

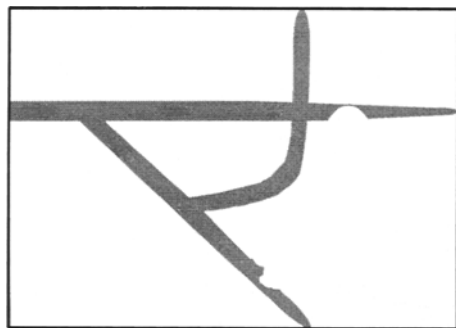
6. Image 2 masked vacuoles, empty regions and some bright background regions. Images with too many hyphae overlapping may cause additional difficulties in identifying vacuoles as shown in the additional illustration. Filter VAC was used to identify vacuoles by a combination of size and shape filters. The very large regions were identified for elimination by an erosion operation. Then size and shape measurements were performed to remove the remaining unwanted regions.



7. Many small background artefacts with similar shape and size to vacuoles as shown in this diagram could not be removed by filter VAC. This diagram shows these small background regions outside the hyphae.



8. Filter HYPV was applied to remove the small non-vacuoles regions from the image. HYPV used the image that contains hyphae alone as a mask to enable artefacts outside the hyphae to be removed from the image. The image shown in step 2 was combined with that of hyphae alone. The smaller background regions were then eliminated by an erosion operation. An image was then reconstructed which contained hyphae and vacuoles.

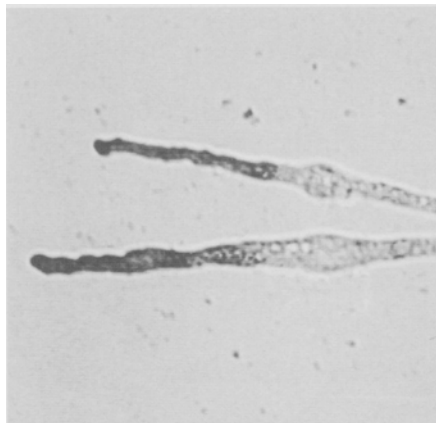


9. The difference between the combined image and the image containing the hyphae alone gave the vacuoles and empty regions.

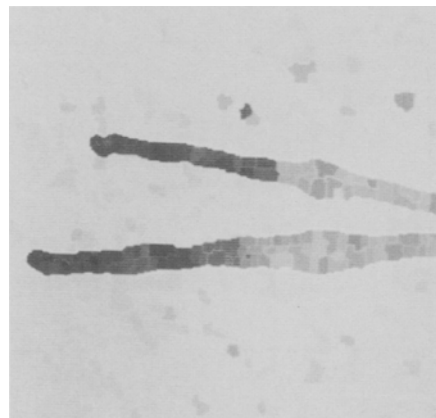


Phase III.
Identification and separation of growing regions

10. The growing regions in the hyphae show darker than the rest of the cytoplasmic regions. Identification and separation of these regions were achieved by a routine or filter called TIP. Some grey processing operations were applied to improve the original image. Firstly, the halos around the boundaries were identified for removal by a top hat operation (see Sect. 2.2). The result of this step is not shown here.



11. The greyness levels of the image were modified by a watershed operation (see Sect 2.2). This divided the whole image into tiny zones each having a uniform grey intensity. The zones are surrounded by single pixel width dividing lines. Watershedding resulted in a much clearer distinction between the growing regions and the rest of the hyphae.



12. The growing regions were then picked out using a detection level which identified all the zones darker than that level, and gave a binary image of the selected zones. Because of the watershed these were separated by dividing lines one pixel wide. Neighbouring zones were then joined together into groups by a closing operation, each masking a growing region of the hyphae. Smaller isolated zones, probably artefacts, were removed by a size filter.

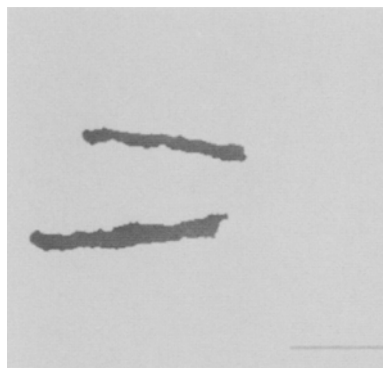


Figure 27b-d shows the binary images of vacuoles and empty regions, hyphae including vacuoles and empty regions (whole hyphae), and the growing regions corresponding to the grey image shown in Fig. 27a. The time of analysis of a sample varied between 25 and 35 min depending on the type of samples and the extent of manual editing required. Following the measurement of all the fields of view, the volumetric proportions of the growing and non-growing cytoplasmic regions (by subtraction of growing regions, and vacuoles and empty regions from total hyphae), and vacuoles and empty regions were obtained. Distributions of different parameters, e.g. vacuole volume, vacuole circularity, were obtained and mean widths and distributions of all the different regions were also found. The degenerated regions were estimated from the distribution of vacuole volume. It was found that vacuoles approximately larger than $30 \mu\text{m}^3$ in volume constitute the degenerated regions of the hyphae [8]. The volume proportions of the degenerated regions were estimated. From the proportions by volume of these four regions, the amount of biomass in each was found using hyphal density values from the literature [52]. The classification of the four regions is shown in Fig. 28.

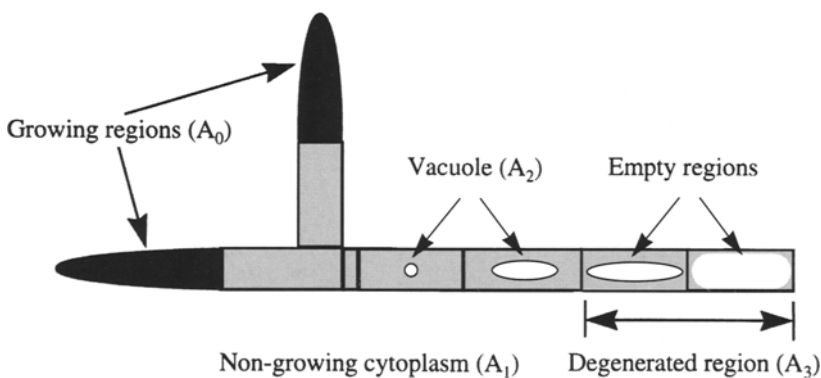


Fig. 28. The regions of hyphal differentiation measured by image analysis [8]

Table 9 gives the results for a sample taken from a fed-batch *P. chrysogenum* fermentation illustrating the information generated by the image analysis method on a typical sample. Figures 29 and 30 show the distributions of vacuole volume and vacuole circularity for a number of fermentation samples across a fed-batch fermentation. The cumulative distribution of vacuole volumes for three samples (Fig. 31) shows the increasing proportion of larger vacuoles with the duration of fermentation.

Figure 32 represents the time profile of the volume proportions of growing regions, and vacuoles and empty regions of a fed-batch *P. chrysogenum* fermentation in which the glucose feed rate was switched between a high and a low value (see Fig. 33). The time course of the cell dry weight, estimated biomass concentrations of the different regions, the volumetric concentration of small vacuoles (volume $\leq 30 \mu\text{m}^3$), and the penicillin titre for the same fermentation are shown in Fig. 33. It can be seen from Figs. 32 and 33 that when the feed rate was reduced there was an increase in both penicillin production and non-growing regions and a decrease in growing regions. This suggests that by switching to a low feed rate some of the growing regions converted to non-growing regions. The results from this fermentation demonstrate the potential of this technique for obtaining better understanding of the penicillin fermentation, particularly the relationship between productivity and differentiation. Clearly, physiological changes caused by manipulating nutrient conditions could be monitored by image analysis.

Table 9. Summary of image analysis results for a *P. chrysogenum* sample taken from a fed-batch fermentation at 72 h [8]

Number of fields analysed	64
Total analysis time (min)	27
Number of features measured:	
Hyphae (total number of mycelial particles)	57
Vacuoles	1740
Growing regions	181
Measured area (μm^2):	
Growing regions	45850 (20 %)
Non-growing regions	142140 (62 %)
Vacuoles	41270 (18 %)
Total	229260
Calculated mean width (μm):	
Growing regions	3.40
Non-growing regions (whole particle)	4.05
Vacuoles	3.80
Calculated volume (μm^3):	
Growing regions	138400 (19 %)
Non-growing regions	480740 (66 %)
Vacuoles	109260 (15 %)
Estimated biomass (g cell dry weight l^{-1} broth):	
Growing regions	5.1 (22 %)
Non-growing regions	15.1 (66 %)
Degenerated regions	2.8 (12 %)
Total	23.0

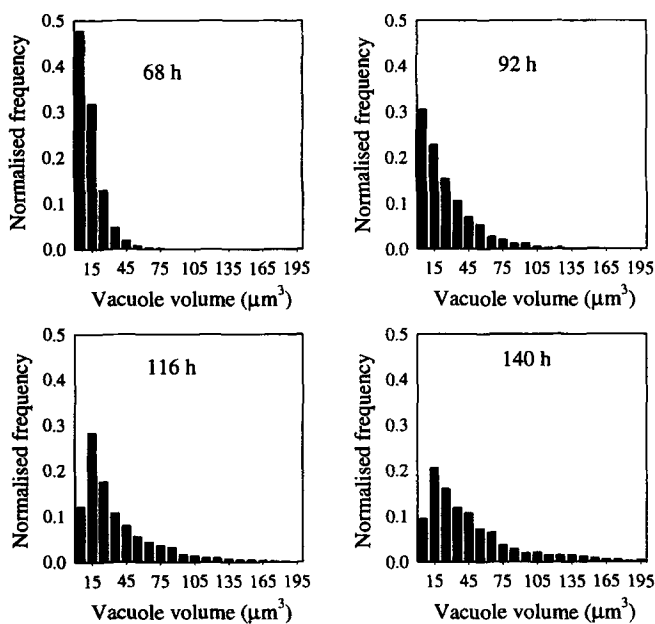


Fig. 29. Distribution of vacuole size during the production phase of fermentation using a defined medium and inoculated with spore inoculum

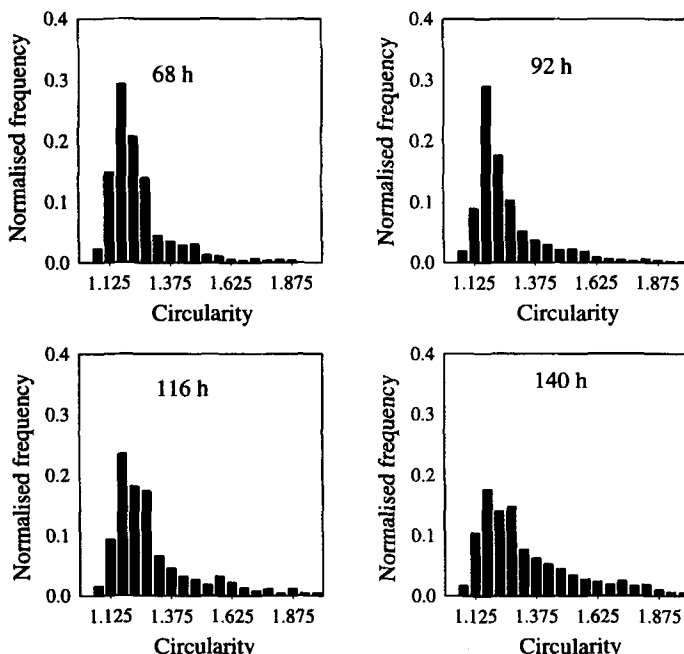


Fig. 30. Distribution of vacuole shape (circularity parameter) for four samples across a fed-batch penicillin fermentation

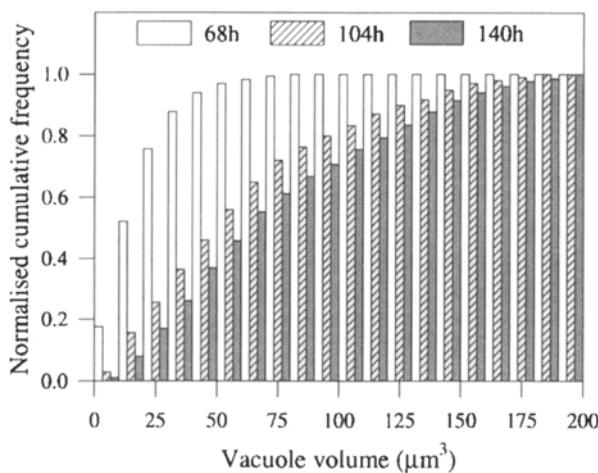


Fig. 31. Cumulative distribution of vacuole volume for three fermentation samples during the production phase [7]

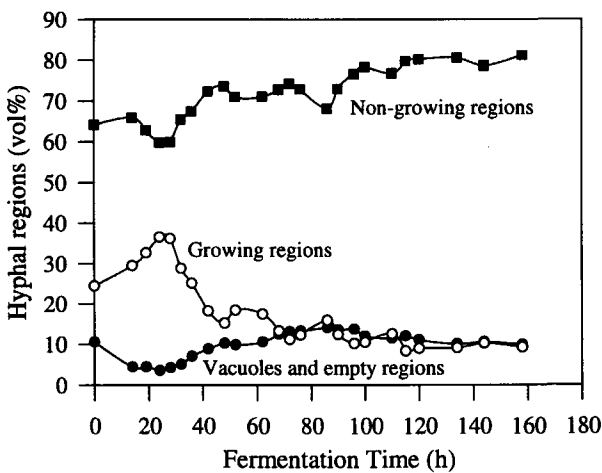


Fig. 32. Time profile of the proportions of different hyphal regions during a fed-batch penicillin fermentation. The glucose feed rate was pulsed during the production phase (see Fig. 33)

Besides characterising differentiation, the method provided other information such as mean widths of various regions that may be important for detailed investigation and modelling of fermentation processes. Figure 34 shows the time profiles of the mean width of hyphae, growing regions, and vacuoles and empty regions of the same fermentation presented in Figs. 32 and 33.

Based on the information of simple differentiation obtained by image analysis a structured model was developed [17]. With a number of fed-batch fermenta-

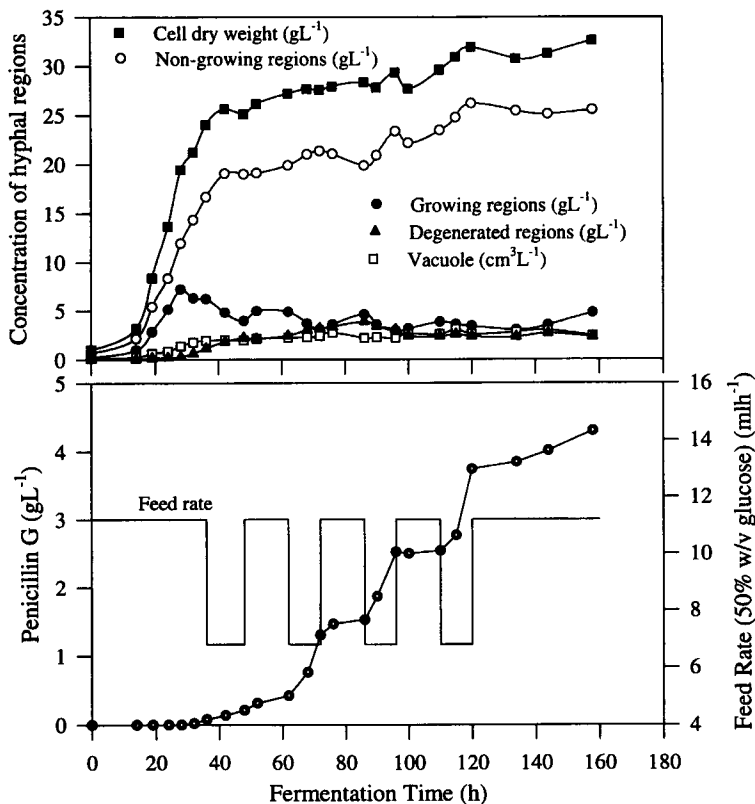


Fig. 33. Time profiles of the concentrations of different hyphal regions corresponding to the fed-batch penicillin fermentation shown in Fig. 32

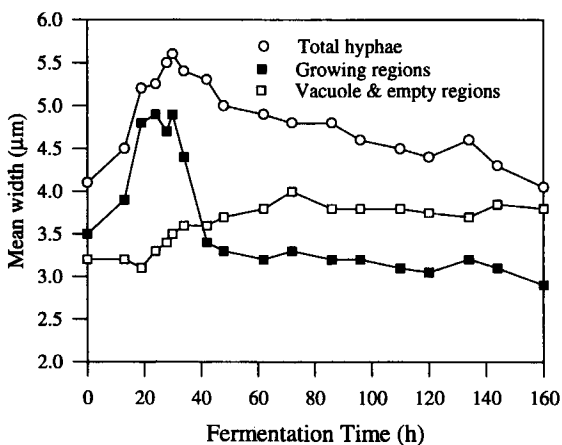


Fig. 34. Time profiles of the mean width of total hyphae, growing regions, and vacuoles and empty regions of the fed-batch fermentation of Fig. 32

tions using different feeding profiles, the model appeared to show good prediction capabilities for the penicillin process.

Recently, an image analysis method has been developed for a more detailed characterisation of differentiation of *P. chrysogenum* [53]. Using colour image processing and a differential staining technique, six physiological states of hyphal regions were identified and separated. Although the method is very slow in its present form for routine laboratory analysis, it provides better physiological understanding of the process. The image analysis method for this characterisation is described in Chap. 2 × (M.N. Pons), with discussion of its future potential. It is probable that new developments in characterisation of mycelial differentiation by image analysis will arise through exploitation of such novel, and particularly multiple, staining techniques.

4

Conclusions

Growth of mycelial microorganisms and their interactions with the environment in the fermenter are complex. Morphology and differentiation are very important reflections of the organism physiology, which change during the course of fermentations as well as with operating conditions. Image analysis is a vital tool to gather data on these aspects of the physiology, and to relate them to fermentation conditions. Furthermore, mathematical modelling of mycelial fermentations needs good data on morphology and physiology, and image analysis is the way to acquire such information.

5

References

1. Oliver SG, Trinci APJ (1985) Modes of growth of bacteria and fungi. In: Bull AT, Dalton H (eds) Comprehensive Biotechnology, vol. 1. Pergamon, p 159
2. Ujcová E, Fencl Z, Musílková M, Seichert L (1980) Biotechnol Bioeng 22:237
3. Paul GC, Priede M, Thomas CR. (1996) Quantitative morphology and physiology of *Aspergillus niger* in submerged citric acid fermentations. Proceedings of the 1st European Symposium on Biochemical Engineering Science, 19–21 September, 1996. Dublin, Ireland, p 168
4. Bartnicki-Garcia S (1973) Sym Soc Gen Microbiol 23:245
5. Zalokar M (1959) Am J Bot 46:555
6. Zalokar M (1959) Am J Bot 46:602
7. Paul GC, Kent CA, Thomas CR (1992) Trans IChemE (Part C) 70:13
8. Paul GC, Kent CA, Thomas CR (1994) Trans IChemE (Part C) 72:95
9. Spassova D, Vesselinova N, Gesiieva, R (1991) Actinomycetes 2:18
10. Lendenfeld T, Ghali D, Wolsehek M, Kubicek-Pranz EM, Kubicek CP (1993) J Biological Chemistry 268:665
11. Adams HL, Thomas CR (1988) Biotechnol Bioeng 32:707
12. Packer HL, Thomas CR (1990) Biotechnol Bioeng 35:111
13. Tucker KG, Kelly T, Delgrazia P, Thomas CR (1992) Biotechnol Prog 8:353
14. Cox PW, Thomas CR (1992) Biotechnol Bioeng 39:945
15. Paul GC, Kent CA, Thomas CR (1993) Biotechnol Bioeng 42:11
16. Smith GM, Calam CT (1980) Biotechnol Lett 2:261
17. Paul GC, Thomas CR (1996) Biotechnol Bioeng 51:558

18. Thomas CR (1992) Trends in Biotechnol 10:343
19. Vecht-Lifshitz SE, Ison AP (1992) J Biotechnol 23:1
20. Thomas CR, Paul GC (1996) Current Opinion in Biotechnology 7:35
21. Metz B, de Bruijn EW, van Suijdam JC (1981) Biotechnol Bioeng 23:149
22. Ramm P (1994) J Neuroscience Methods 54:131
23. Paul GC (1993) Image analysis for characterising *Penicillium chrysogenum* differentiation, PhD thesis, University of Birmingham, UK
24. Klein JC, Collange F, Bilodeau M (1989) Programmable logic cell arrays: a new technology for image analysis. Cambridge Instrument Ltd, Cambridge, UK
25. Russ JC (1990) Computer assisted microscopy. The measurement and analysis. Plenum, New York
26. Serra J (1982) Image analysis and mathematical morphology. Academic Press, London
27. Paul GC, Kent CA, Thomas CR (1993) Binary 5:92
28. Reichl U, Buschulte TK, Gilles ED (1990) J Microsc 158:55
29. Paul GC, Thomas CR (1995) An image processing algorithm for characterising mycelial aggregates grown in submerged fermentation. Proceedings of the 4th International Quantimet and Stereoscan User Conference, 2–5 Oct. 1995, Madingley Hall, Cambridge, UK
30. Paul KR, Paul GC, Thomas CR (1995) Effect of spore inoculum concentration on morphology of *Streptomyces clavuligerus*. Proceedings of the 1995 IChemE Research Event – First European Conference for Young Researchers in Chemical Engineering, 5–6 January, 1995, Edinburgh, UK, p 980
31. Tucker KG, Thomas CR (1992) Biotechnol Lett 14:1071
32. Tucker KG, Thomas CR (1994) Biotechnol Techniques 8:153
33. Galbraith JC, Smith JE (1969) Trans Brit Mycol Soc 52:237
34. Paul GC, Thomas CR (1995) Effect of fermentation medium on the morphology of *Penicillium chrysogenum* in submerged fermentation. Proceedings of the 1995 IChemE Research Event – First European Conference for Young Researchers in Chemical Engineering, 5–6 January, 1995, Edinburgh, UK, p 974
35. Paul GC, Kent CR, Thomas CR (1994) Biotechnol Bioeng 44:655
36. Nielsen J, Johansen CL, Jacobsen M, Krabben P, Villadsen J (1995) Biotechnol Prog 11:93
37. Prosser JI, Trinci APJ (1979) J Gen Microbiol 111:153
38. Prosser JI, Tough AJ (1991) Crit Rev Biotechnol 10:253
39. Nielsen J, Krabben P (1995) Biotechnol Bioeng 46:588
40. Yang H, Reichl U, King R, Gilles ED (1992) Biotechnol Bioeng 39:44
41. Yang H, King R, Reichl U, Gilles ED (1992) Biotechnol Bioeng 39:49
42. Reichl U, King R, Gilles ED (1992) Biotechnol Bioeng 39:164
43. Durant G, Crawley G, Formisyn P (1994) Biotechnol Techniques 8:395
44. Durant G, Cox PW, Formisyn P, Thomas CR (1994) Biotechnol Techniques 8:759
45. Pichon D, Vivier H, Pons MN (1993) Growth monitoring of filamentous microorganisms by image analysis. In: Karim MN, Stephanopoulos, G (eds), Modeling and control of biotechnological processes. Pergamon, p 307
46. Edelstein L, Hadar Y (1983) J Theor Biol 105:427
47. Tough AJ, Pulham J, Prosser JI (1995) Biotechnol Bioeng 46:561
48. Deo YM, Gaucher GM (1984) Biotechnol Bioeng 26:285
49. Mou D-G, Cooney CL (1983) Biotechnol Bioeng 25:225
50. Paul GC, Thomas CR (1996) A mathematical model of swelling and germination of fungal spores in inoculum cultures. Proceedings of the 5th World Congress of Chemical Engineering, 14–18 July, 1996, San Diego, CA, p 717
51. Packer HL, Keshavarz-Moore E, Lilly MD, Thomas CR (1992) Biotechnol Bioeng 39:384
52. Nestaas E, Wang DIC (1983) Biotechnol Bioeng 25:781
53. Vanhoutte B, Pons MN, Thomas CR, Louvel L, Vivier H (1995) Biotechnol Bioeng 48:1